Polymer Brushes in Restricted Geometries: Structure and Lubricity

By

DENNIS JOHN MULDER
B.S. (University of California, Davis) 1999
M.S. (University of California, Davis) 2006
M.B.A. (University of California, Davis) 2006

DISSERTATION

Submitted in partial satisfaction of the requirements for the degree of

DOCTOR OF PHILOSOPHY

in

Chemical Engineering

in the

OFFICE OF GRADUATE STUDIES

of the

UNIVERSITY OF CALIFORNIA

DAVIS

Approved:

_____
Tonya L. Kuhl, Chair

_____
Timothy E. Patten

_____
Roland Faller

Committee in Charge
2011

ProQuest LLC.
789 East Eisenhower Parkway
P.O. Box 1346
Ann Arbor, MI 48106 - 1346

Chapter 1: Opposing Polymer Brushes in Confinement

Based on Mulder, D.J. and Kuhl, T.L., Polymer Brushes In Restricted Geometries. ***Soft Matter***, 2010, **6**, 5401-5407

Abstract

The structure of polymer brushes has been the subject of considerable theoretical and experimental activity. Experimental measurements of the steric forces between grafted brushes and the structure of a single brush at the solid-solution interface are in good agreement with theoretical predictions. However, the physical structure brush layers adopt under confinement has remained elusive. In this chapter, we report measurements of polymer brush density distributions in good solvent as a function of compression. The extension and interpenetration of the brushes are unambiguously determined using neutron reflectivity and contrast matching techniques. The measurements reveal a significant increase in brush concentration at the grafting surface with compression. This is in contrast to theoretical predictions of uniform density distributions as polymer brushes are compressed. The low interpenetration and brush compaction at the anchor surface provides new insight into why such layers are so effective at reducing friction and wear between surfaces.

Introduction

Knowledge of the conformations of terminally anchored polymer chains under confinement and/or in solvent flow is essential for predicting their interaction forces and tribological and rheological properties [1-4]. The equilibrium properties of uncompressed polymer brush layers predicted by self-consistent field theory and simulations have been

confirmed by a number of experiments primarily utilizing scattering techniques [1-7]. Much less well understood is the structure such brushes adopt during compression and confinement (Figure 1-1). Although force spectroscopy techniques such as the Surface Force Apparatus[8-10] and various Scanning Probe Microscopies [11, 12] have been very useful in quantifying the interaction forces between polymer layers, these techniques are indirect in that interaction forces are measured and structure is inferred. As a result, much of our understanding of the structure and behavior of brushes in confined geometries has evolved from modeling approaches. These include scaling theories, analytical and numerical statistical models, and Monte Carlo and molecular dynamics simulations. An advantage of modeling approaches is that system parameters such as grafting density, solvent quality, and adsorption strength to the grafting surface can be easily varied allowing their effects to be investigated and polymer brush behavior predicted [4, 13-17]. However, the interpenetration of polymer brushes has received much less attention both experimentally and theoretically [15-19]. This is due to the difficulty of extracting polymer conformations in restricted geometries and brush interpenetration becomes negligible in the limit of infinite chain length. Molecular simulations and self-consistent mean field approaches (typically, chains<100 monomers are studied) predict significant brush interpenetration with compression [4, 13, 15, 16, 20-23].

On the experimental side, neutron reflectivity measurements are exceptionally well suited for studying confined polymer brush layers because; the neutron's weak interaction allows it to penetrate matter to probe structure at buried interfaces, long term neutron exposure does not result in radiation damage or significant activation of polymers, and the scattering length density (SLD) of the polymer and solvent can be

easily manipulated by replacing hydrogen atoms with deuterium to adjust the films contrast with the surrounding medium (e.g. to mask or highlight it) without significantly altering chemical properties [24]. Thus, by judious selection of contrast, neutron reflectivity can be used to non-invasively determine the density and extension of a polymer brush film on one surface as it is compressed by an opposing brush, e.g. Figure 1-1.

Neutron reflectivity and contrast masking techniques were thus used to determine the density distribution of high grafting density polymer brushes in good solvent conditions at a single surface and how the proximity of a second brush alters the brush conformation as a function of compression. Our experimental results are compared to theoretical predictions.

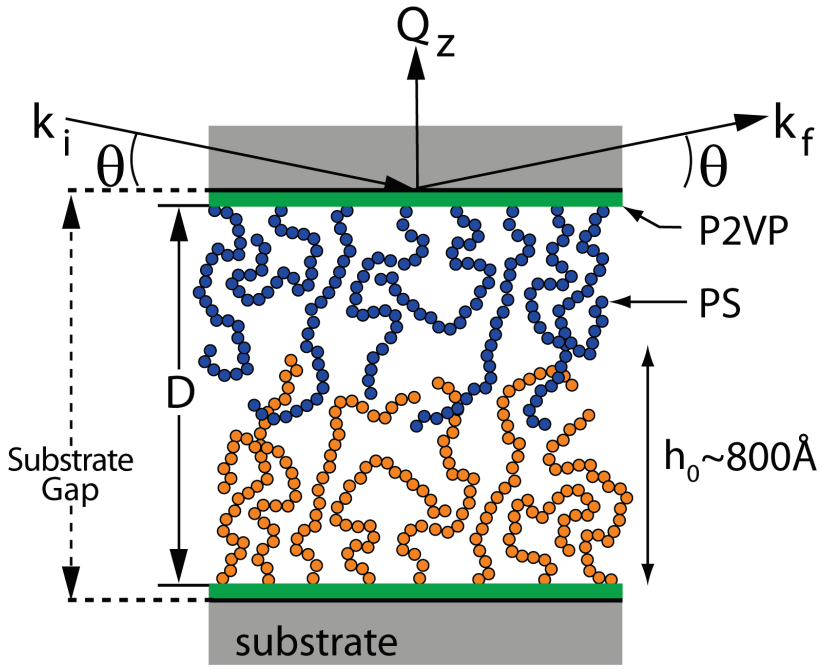

Figure 1-1 Geometry of the neutron reflectivity measurements and experimental system.

Experimental

Sample Preparation

High density polymer brushes were created using 50:50 polystyrene-poly-2-vinylpyridine diblocks (PS-P2VP). The P2VP portion of the diblock was hydrogenated while the PS portion was either hydrogenated (hPS-P2VP MW=122k, polydispersity = 1.11, fraction P2VP = 0.51) or perdeuterated (dPS-P2VP MW=136k, polydispersity = 1.10, fraction P2VP = 0.52) to take advantage of contrast labeling. Uniform PS-P2VP thin-films were prepared by spin coating at 2000 rpm for 30 seconds on dry, ultra-clean substrates in a clean room environment. The substrates were either Silicon, Quartz, or Sapphire to provide different contrasts. For the work reported, the spin-coating solution was 6 mg/ml PS-P2VP dissolved in toluene by continuous stirring for at least 24 hours in advance. Different brush grafting densities can be prepared by changing the solution concentration. The solution was filtered a minimum of 3 times through 0.45μm PTFE filters just prior to use. After spin-coating, the polymer thin-films were annealed under vacuum at 180°C for 24 hours and cooled to room temperature before removal. The glass transition temperature for both polymers is just over 100°C. The polymer film forms an equilibrium alignment of lamellae parallel to the substrate as P2VP prefers to wet the hydrophilic substrate while PS segregates to the air interface [3].

Neutron Reflectivity

Neutron reflectivity measurements were performed on the time-of-flight SPEAR beamline at the Manuel Lujan Neutron Scattering Center, Los Alamos National Laboratory. The range of neutron wavelengths was λ=2-16Å. The measured Q_z range was from 0.008 to about 0.2Å^{-1} and reflectivities, R, with reasonable statistics were

obtained to values of R~10^{-6}. The data were reduced and plotted as RQ_z^4 versus Q_z compensating for a sharp Q_z decrease of the reflectivity due to Fresnel's law. The error bars on the data represent the statistical errors in the measurements (standard deviation, σR) where the uncertainty in the Q_z resolution, $\sigma Q_z/Q_z$, was nearly constant over this scattering vector range with a value of ~3%.

The fitting program used for this data is an integral data collection and profile modeling analysis package for the MIRROR neutron reflectometer developed by W.A. Hamilton and J.B. Hayter (1992-2003). The MIRROR program calculates reflectivity using the optical matrix method from boxes of constant thickness and scattering length density. The statistical and error estimation concepts used therein are described in P.R. Bevington Data Reduction and Error Analysis for the Physical Sciences (McGraw-Hill, New York, 1969) Chapter 11 and in W.H. Press, S.A. Teukolsky, W.T. Vetterling and B.P. Flannery, Numerical Recipes in Pascal (Cambridge University Press, Cambridge, 1989), Chapter 15. The minimization routine employed by the MIRROR program is the "downhill simplex" method of J.A. Nelder and R. Mead, Computer Journal **7**, 308 (1965), in an implementation described in Chapter 10.4 of Numerical Recipes in Pascal. In the absence of a critical edge, an additional parameter to normalize the reflectivity was included.

Neutron Confinement Cell

The effect of confinement and compression of opposing, high grafting density PS polymer brushes was investigated using the Neutron Confinement Cell (NCC), Figure 2-1 [25]. The NCC allows control of the surface separation and parallel alignment of the substrates under applied loads – with *in situ* structural characterization of the intervening

material using neutron reflectivity measurements. The heart of the NCC is the substrates used to confine the system of interest. Theoretically, the minimum gap obtainable with the device is solely a function of the smoothness (waviness) of the substrates used. In other words, the gap separation is equivalent to the separation between the two substrates. In the current experiments, 50mm diameter, 15mm thick, single crystal substrates of optical flatness less than $\lambda/25$ at 632.8nm over the inner 90% of the surface were used. The outer 10% of each substrate was rounded off to ensure that there were no edge asperities. The NCC maintains substrate alignment at a constant gap separation for the duration of the reflectivity measurement (2 to 12 hours). Otherwise, contributions from different substrate separations will tend to smear out the reflectivity profile [26, 27]. The substrates are mounted into recesses within the steel housing machined to a lapped tolerance of less than 0.25 . A Teflon gasket material of Durlon 9000 is placed along the bottom and sides of the substrate recesses to distribute the applied load evenly across the substrate surface. The flexibility of the gasket material and the compliance of the substrate materials enable the surfaces to conform and self align. Gap separations of less than 1000Å can be obtained using this construction. The assembled device fits on top of a piston ram, which can be used to apply large normal loads to the substrates through a series of variable spring constant Belleville washers. By measuring the deflection of the Belleville washers, the applied load can be accurately determined. However, the presence of a single, small particle between the surfaces dominates the force, and has so far precluded a measurement of the brush interaction force during NCC measurements. Comparisons to polymer brush force profiles in the literature can still be done based on the separation between the surfaces [8-10, 26, 27].

Results and discussion

For these studies, very high grafting density brushes were created by spin-coating 50:50 diblocks of polystyrene-poly-2-vinylpyridine (PS-P2VP) on single crystal substrates. The polystyrene portion of the diblock was either hydrogenated (hPS, MW 122k) or deuterated (dPS, MW 136k). The films were annealed significantly above the glass transition tempterature of both blocks to induce segregation; the P2VP layer wets the substrate and the PS portion goes to the air interface [3, 28]. The prepared polymers were first characterized in the dry state. Typically films of 250-300Å were used.

Single surface control measurements

An example neutron reflectivity profile of an annealed dPS-P2VP layer on quartz in air is shown in Figure 1-2. Specular reflectivity measured as a function of momentum transfer, $Q_z = (4\pi \sin\theta)/\lambda$, provides information on the average scattering length density normal to the substrate and can be used to determine the concentration of atomic species at a particular depth in the film. Visible fringes in the reflectivity profile arise from interference between waves being reflected from the different interfaces in the sample. From the measured reflectivity profile, the SLD's, thicknesses, and roughness of the layers can be determined by modeling the SLD profile and iterating to minimize the difference between the measured reflectivity profile and that obtained from the modeled SLD profile. For the simple case of a PS-P2VP film in air, boxes of constant thickness and SLD were used to model the PS and P2VP portion of the thin-film polymer layer. Interfaces were smeared with an error function. The fitted SLD profile (Figure 1-2) indicates the polymer layers are well segregated with an interfacial roughness of about 10Å and a surface mass coverage of 13.6 mg/m^2 of PS.

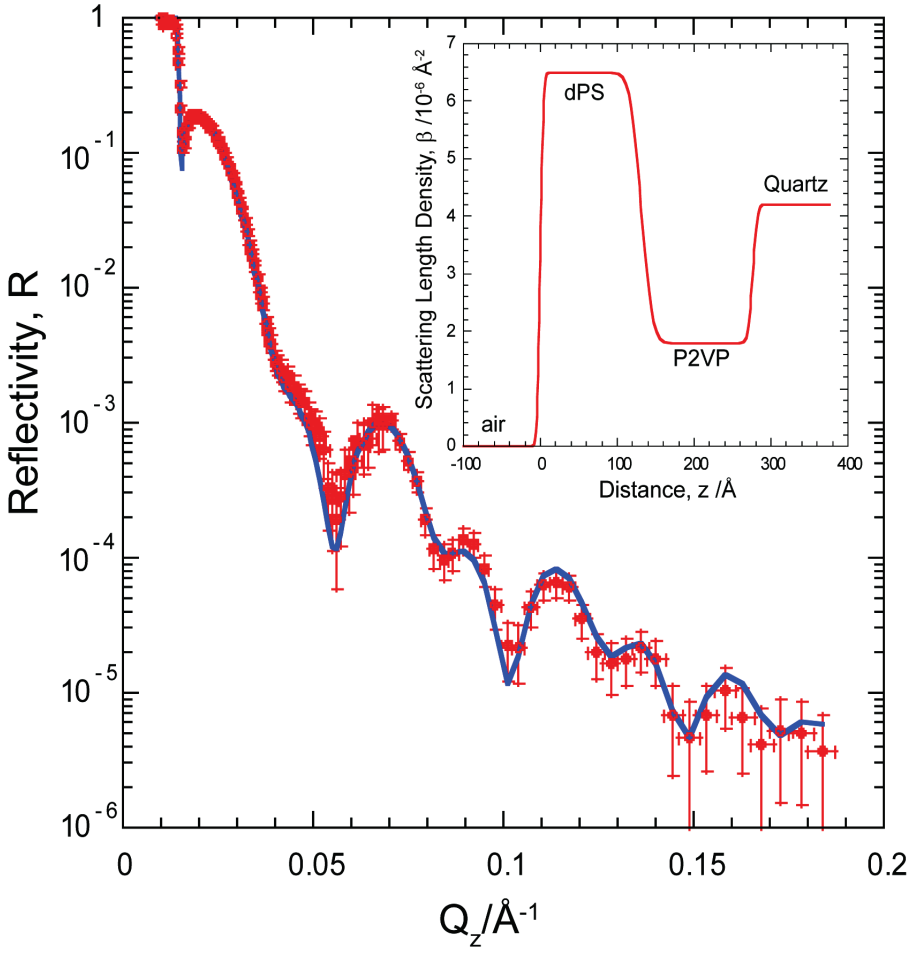

Figure 1-2 Reflectivity profile of a single dPS–P2VP layer on a quartz substrate. The solid curve is a fit to the data based on the SLD profile (inset).

In a good, selective solvent, here toluene, the P2VP block anchors the chain to the oxide substrate while the PS block extends away from the interface into the solution (Figure 1-1). At a single surface, the extension of the PS brush layer and its density distribution is dictated by the chain grafting density, σ_G. For example, at low grafting densities ($\sigma^* \leq 1$,where $\sigma^* = \sigma_G \pi R_F^2$ is the reduced surface density and R_F is the Flory radius) the chains are sufficiently far apart that they can adopt coiled conformations, and

are in the so-called "mushroom regime". The height of the brush in a good solvent scales approximately as the Flory radius, $N^{3/5}$ [17]. The semi-dilute brush regime occurs at somewhat higher grafting densities ($\sigma^* \geq 1$). These types of films have been the most studied. In the semi-dilute regime, the brush height scales as ${N\sigma_G}^{1/3}$ and both theory and simulations predict a parabolic density profile away from the surface (Eq 1-1, $n = 2$) with an exponential tail [17]. With increasing grafting density, the brush profile is predicted to flatten and follow a higher order power law [3], ($n > 2$),

$$\phi(x) = \phi_0 \left(1 - \left(\frac{x}{h_0}\right)^n\right) \qquad \textbf{Equation 1-1}$$

where ϕ_0 is the volume fraction of the brush at the interface and h_0 is the unconfined, equilibrium extension of the brush perpendicular to the interface.

Figure 1-3 shows the reflectivity profile of a solvated P2VP-PS brush, $\sigma^* \approx 30$. The corresponding SLD model used to fit the data is based on Eq 1-1 - a power law extending from the P2VP layer (Eq 1-2). To account for the polymer tails extending into the solvent, this transitions to a reversed power law (Eq 1-3) and then bulk solvent (Eq 1-4). The series of equations (Eq 1-2 through 1-4) recapitulate the theoretical predictions for the polymer density profile at a single surface; yet retain sufficient flexibility to allow a variety of profiles to be obtained as dictated by the data. As will be shown later, these equations also provide a convenient framework for the analysis of opposing polymer brushes under confinement:

$$SLD(0 \leq x \leq h_1) = SLD(0) - \left[SLD(0) - SLD(h_1)\right]\left(\frac{x}{h_1}\right)^n \qquad \textbf{Equation 1-2}$$

$$SLD(h_1 \leq x \leq h_2) = \quad SLD(h_2) + [SLD(h_1) - SLD(h_2)]\left(\frac{h_2 - x}{h_2 - h_1}\right)^n \quad \textbf{Equation 1-3}$$

$$SLD(x \geq h_2) = \quad SLD_{solvent} \quad \textbf{Equation 1-4}$$

where x=0 corresponds to the portion of the brush extending from the P2VP anchor layer, h_1 the endpoint of the first (n_1) power law, and h_2 the endpoint of the second (n_2) reversed power law starting the bulk toluene layer. For clarity these points are labeled in Figure 1-3a.

To obtain the polymer brush density distribution, the SLD profile (Figure 1-3a) was converted to a volume fraction profile using:

$$SLD_{fitted} = \phi_{PS}(SLD_{PS}) + (1 - \phi_{PS})SLD_{toluene} \quad \textbf{Equation 1-5}$$

Even for very high grafting coverages studied here, the unconfined brush density profile (Figure 1-3b) was found to remain parabolic ($n = 2 \pm 0.1$) with an extension of $h_0 \cong$ 800Å and RMS thickness, h_{rms}^0 , of 340Å [16, 29]. An important check of the physical reasonableness of the model fit was verified by conservation of mass where the amount of polymer in the solvated case matched to ±2% of that found in the dry case. Table 1-1 shows the fitting parameters for these control measurements.

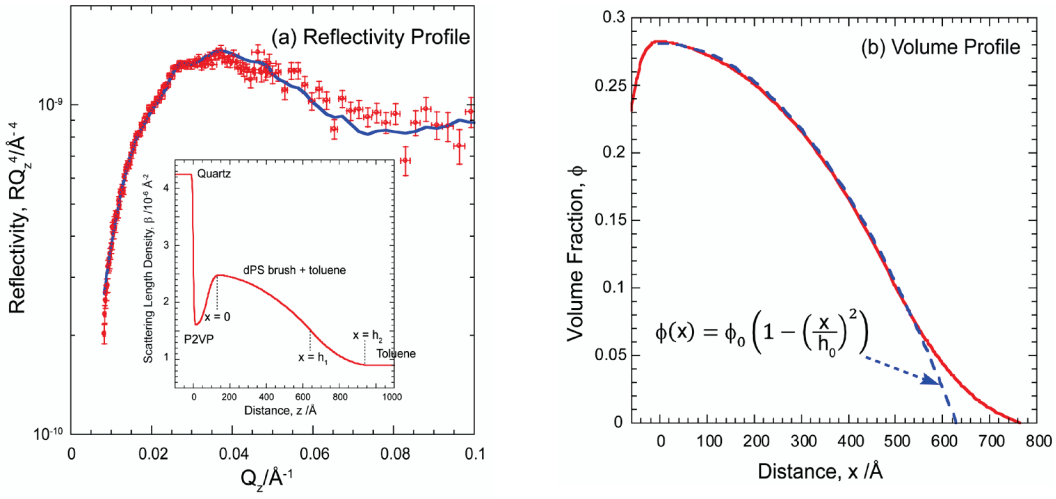

Figure 1-3 (a) Reflectivity profile of an unconfined dPS–P2VP layer on a quartz substrate solvated in h-toluene. The solid curve is a fit to the data based on the SLD profile (inset). (b) Volume fraction profile and power law fit.

Table 1-1 Single Surface Fitting Parameters

												Roughness (Å)		
Solvent	dPS T (Å)		dPS SLD					P2VP T (Å)	P2VP SLD	Q SLD	χ^2	P2VP-PS	Q-P2VP	PS-Air
Air	131		6.5					145	1.80	4.20	2.6	11	5	3
h-Toluene	h_1 (Å)	h_2 (Å)	$SLD(0)$	$SLD(h_1)$	$SLD(h_2)$	n_1	n_2							
Small	570	330	2.5	1.5	0.9	2.0	2.0	75	1.60	4.20	1.6	28	5	

Opposing Symmetric Polymer Brush Measurements in Air

In Figure 1-4, the neutron reflectivity profile and fitted scattering length density (SLD) profile obtained from opposing polymer layers in air (non-solvated state) are shown. The high frequency Keissig fringes at low Q_z clearly indicate that the gap spacing between the substrates is quite small, 2π / fringe spacing ≈ 1000 Å. However, the relatively low visibility of the fringes indicates there is some variation in separation across the gap. Although the surfaces are parallel, small variations in the substrate gap spacing, $(T - T_{avg})$, add independently to the total reflected signal if they are larger than the coherence length of the neutron beam ~1μm [25, 28]. As the beam footprint is about 1.5 square centimeters, this is not unexpected. To account for this, the reflectivity was calculated by incoherently averaging over the range of gap spacings, assuming a Gaussian variation, σ, using:

$$R(Q_Z, T_{avg}) = \frac{1}{\sigma\sqrt{2\pi}} \int R(Q_Z, T)\, e^{-\frac{(T-T_{avg})^2}{2\sigma^2}} dT \qquad \textbf{Equation 1-6}$$

In both Figures 1-4a and b, the same SLD model (Figure 1-4c) was used to generate the solid curve fits to the reflectivity profile. In Figure 1-4b, however, the visibility of the fringes was reduced by incoherently averaging the gap spacing (Equation 1-6) with a Gaussian standard deviation of 65Å over the sampled area.

The inter-substrate region was modeled as two layers (P2VP and PS) mirrored across the midpoint. Assuming this region is symmetric greatly decreases the number of fitting parameters and computational time. Parameters from the SLD model are provided in the Table 1-2. The fitted scattering length densities match well to theoretical values, and the thickness of the PS-P2VP lamellae matches well to ellipsometry measurements

conducted just after spin-coating the layers and to the results on a single substrate, Figure 1-2. In this case, the total amount of polymer deposited on each substrate was Γ=12.6 mg/m^2 or 120Å PS film thickness.

Table 1-2 Opposing Symmetric Polymer Brush Fitting Parameters

Solvent	D (Å)	dPS T (Å)		dPS SLD				
Air	1110	120		6.4				
h-Toluene		h_1 (Å)	h_2 (Å)	$SLD(0)$	$SLD(h_1)$	$SLD(h_2)$	n_1	n_2
Small	933	329	430	2.88	2.16	1.7	2.7	2.0
Medium	969	329	430	2.81	1.99	1.7	2.5	2.0
Large	1000	330	430	2.74	1.86	1.6	2.4	2.3

Solvent	P2VP T (Å)	P2VP SLD	Si SLD	SiO_2 T (Å)	SiO_2 SLD	S SLD
Air	130	1.90	2.10	10	3.50	5.65
h-Toluene						
Small	120	1.60	2.10	15	3.51	5.76
Medium	120	1.60	2.10	13	3.54	5.68
Large	120	1.60	2.10	14	3.54	5.69

			Roughness (Å)				
Solvent	χ^2	Incoh (Å)	P2VP-PS	Si-SiO_2	SiO_2-P2VP	P2VP-S	PS-Air
Air	2.4	65	45	4	2	4	2.5
h-Toluene							
Small	2.1	45	15	5	5	5	
Medium	2.4	45	15	5	5	5	
Large	2.5	45	15	5	5	5	

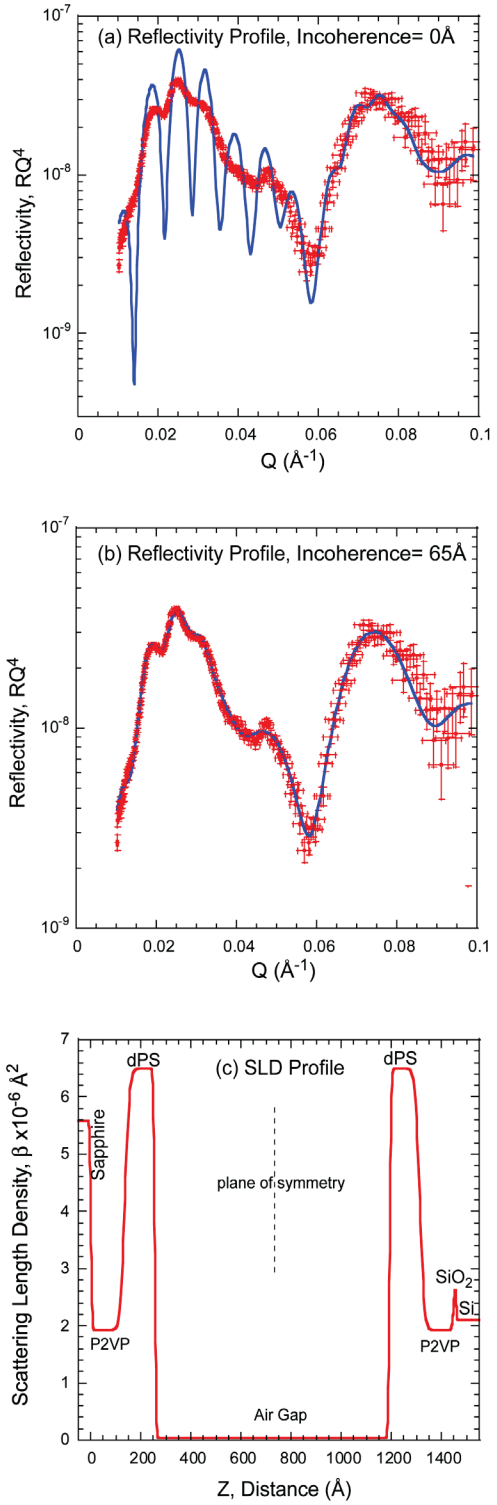

Figure 1-4 (a) Reflectivity profile for opposing spin coated dPS–P2VP layers. The small Q interference peaks in the profile result from constructive interference between the substrates and their overall separation. The higher Q peaks are due to the polymer layers. The solid curve is a fit to the data based on (c) the SLD profile. (b) Reflectivity profile generated by the incoherent averaging of the calculated model reflectivity based on the SLD profile (c) over a 65Å Gaussian distribution of gap thicknesses.

Opposing Symmetric Polymer Brush Measurements in Toluene

Figure 1-5a shows the neutron reflectivity profile after these deuterated PS brushes were solvated in toluene at three different gap separations (1300, 1250, and 1200Å). For this symmetric brush case, the brush region was modeled as three layers similar to the single surface profile but mirrored across the intersubstrate midplane. Equation 1-4 was also modified to account for the brush overlap region:

$$SLD\left(h_2 \leq x \leq \frac{D}{2}\right) = SLD(h_2) \qquad \textbf{Equation 1-7}$$

where D is the distance between the two opposing PS/P2VP interfaces (the PS brush region). To cover the full range of possible brush conformations, the PS brush region SLD was allowed to vary from that of pure h-toluene corresponding to collapse of the brushes to a mixture of PS and h-toluene to account for compression and interpenetration of the brushes. Three different confinement levels are presented. The best fit to the reflectivity data are the solid curves shown in Figure 1-5a. In each case, the quality of fit was very good with $\chi^2 < 3$. The models included incohertent averaging with σ=45Å gap variation.

Figure 1-5c shows the converted volume fraction profiles for the three confiment levels. Notably, the PS volume fraction at the interface *increases* as the brushes are compressed, rather than becoming more flattened and uniform with compression as predicted. The brush profile remained parabolic ($n = 2 \pm 0.5$) and conservation of mass was within 2% of the dry, non-solvated sample. Symmetric dPS brushes enables the total PS volume fraction between the substrates to be quantitatively determined. However, the extension of the each brush can only be estimated from the total volume fraction profile.

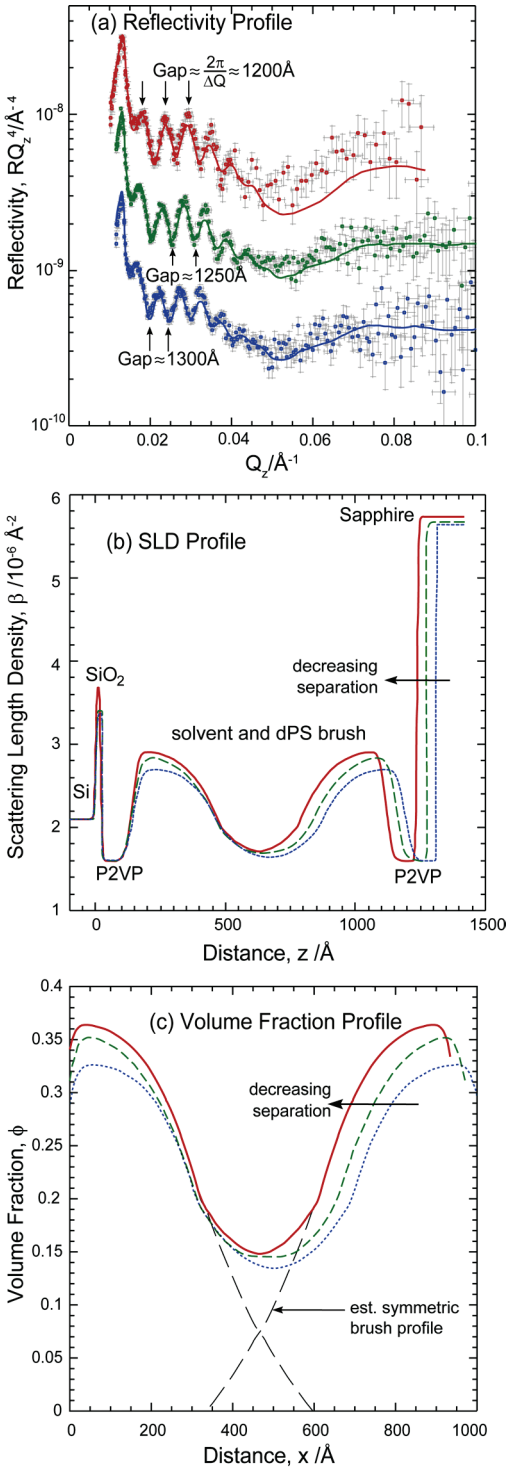

Figure 1-5 Neutron reflectivity data for three different compressions of symmetric dPS brushes in toluene. Deviations in the substrate separation were accounted for by assuming a Gaussian distribution. Solid curves are fits to the data based on the scattering length density (SLD) profiles shown in (b). (c) The corresponding volume fraction profiles for the three compressions. The long dashed lines are estimated extensions of the individual brushes.

Opposing Asymmetric Polymer Brush Measurements

Experiments on asymmetric brushes - one side dPS, the other hPS - provide contrast to determine extension and interpenetration of the brushes under confinement. A mixture of 90% hydrogenated and 10% deuterated toluene has the same neutron scattering density as hPS and thus masks or hides this brush while maintaining high contrast with dPS.

Using this approach, the extension of the dPS brush can be measured explicitly. For example, if the PS brushes interpenetrate with no compression of the brushes, the profile is simply the summation of two uncompressed single layer profiles. In this case, the total polymer density profile will increase in the overlap region and flatten (become more uniform in concentration). Once the density of the overlapping brushes matches that at the anchor surface (P2VP layer), the total PS brush density will increase with decreasing separation between the substrates. Conversely if the opposing brush acts as an impenetrable wall, the density profile of the brush will have the same power law form but increase in concentration with compression dropping abruptly to zero at the edge of the opposing brush.

Control air measurements and best fit models are shown in Figure 1-7. The SLD profile given in Figure 1-7c was modeled similarly to the previous opposing dPS brushes except there was no plane of symmetry. The SLD profile shows an inter-substrate gap separation of about 2500 Å. The NCC was solvated with the 90% hydrogenated and 10% deuterated toluene mixture and load was applied to reduce the separation. Figure 1-8a shows the reflectivity and the best-fit profiles for, $D \approx$ 1440, 1125, and 980 Å corresponding to a reduced separation $\tilde{u} = 0.9$, 0.7, and 0.6, where $\tilde{u} = D/2h_0$. The data

was modeled as the single surface profile with two additional box layers for the opposing P2VP and substrate. The models included incoherent averaging with σ=80Å gap variation. The calculated volume fraction profiles (solid lines) of the dPS brush are shown in Figure 1-8c and selected parameters are summarized in Table 1-3. All fitted parameters are provided Table 1-4. To highlight the interpenetration of the two brushes, the volume fraction of the hPS brush, was assumed to be the mirrored image of the dPS brush on the opposing surface (dashed lines). Although an estimate, the mirrored image is in excellent agreement with the measured symmetric profiles in Figure 1-5.

The amount of interpenetration was determined using [15] (Figure 1-6):

$$I(D) = \int_{D/2}^{D} \phi_1(x)\, dx \Big/ \int_0^D \phi_1(x)\, dx \qquad \textbf{Equation 1-8}$$

For small compressions the brushes weakly interpenetrate and the profile matches well to that measured at a single surface (no confinement). With greater confinement (decreasing substrate separation) the amount of interpenetration increases but the extension of the brush, h, shows a concomitant decrease and the density profile becomes steeper. The level of interpenetration is much less than that of an ideal system where the profile is simply the summation of the two uncompressed single layer profiles (Table 1-3). Rather than becoming more uniform in concentration in the overlap region as the brushes are compressed (decreased substrate separation), the brush density increases at the anchor surface. This behavior can be quantified by the compression parameter, ξ, where $\xi = h_{rms}/h^0_{rms}$, and h^0_{rms} is the root mean squared thickness of the uncompressed brush. At each substrate separation distance, the compression of the brush is found to be in good agreement with numerical self-consistent field theory (NSCF) of Whitmore and

Baranowski [16] (Table 1-3). These first experimental results of brush overlap measurements show that some interpenetration of the brushes occurs with compression as well as an unpredicted increase of brush density at the tethered surface. This finding correlates well with the low friction measured between surfaces bearing grafted polymer brushes in good solvent conditions [9, 15, 19, 30]. Indeed, simulations by Kreer et al. [31], indicated that the shear stress between sliding polymer brushes varies approximately linearly with the interpenetration of the brushes. Measurements of the structure of polymer brushes under confinement during shear are currently being investigated [32].

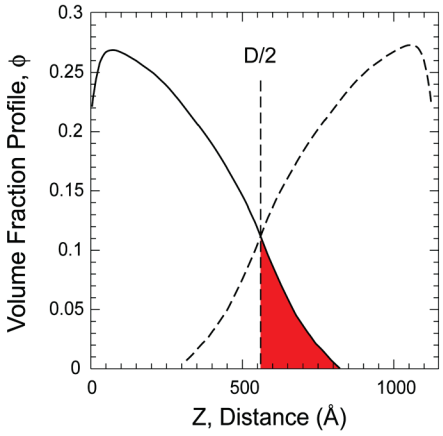

Figure 1-6 Shaded area illustrates calculated amount of interpenetration (Equation 1-8)

Table 1-3 Summary Parameters for Asymmetric Brushes

$\tilde{u}$	ϕ_{max} [§]	h_0/Å	n [ŧ]	ξ [¥]	$I_{exp}(D)$*
Single surface	0.27 ± 0.01	820 ±20	2.0 ±0.1		
0.9	0.26	795	1.7	0.99 (0.98)	0.006 [0.010]
0.7	0.31	705	1.5	0.85 (0.87)	0.029 [0.089]
0.6	0.34	630	1.5	0.78 (0.79)	0.048 [0.162]

*[§]The maximum volume fraction occurs at x=0, Eq 2. [ŧ] The power **n** is obtained by fitting Eq 1-1 to the volume fraction profile.*

*[¥] Compression parameter prediction ( ) from Whitmore and Baranowski [16]. * Full interpenetration [ ].*

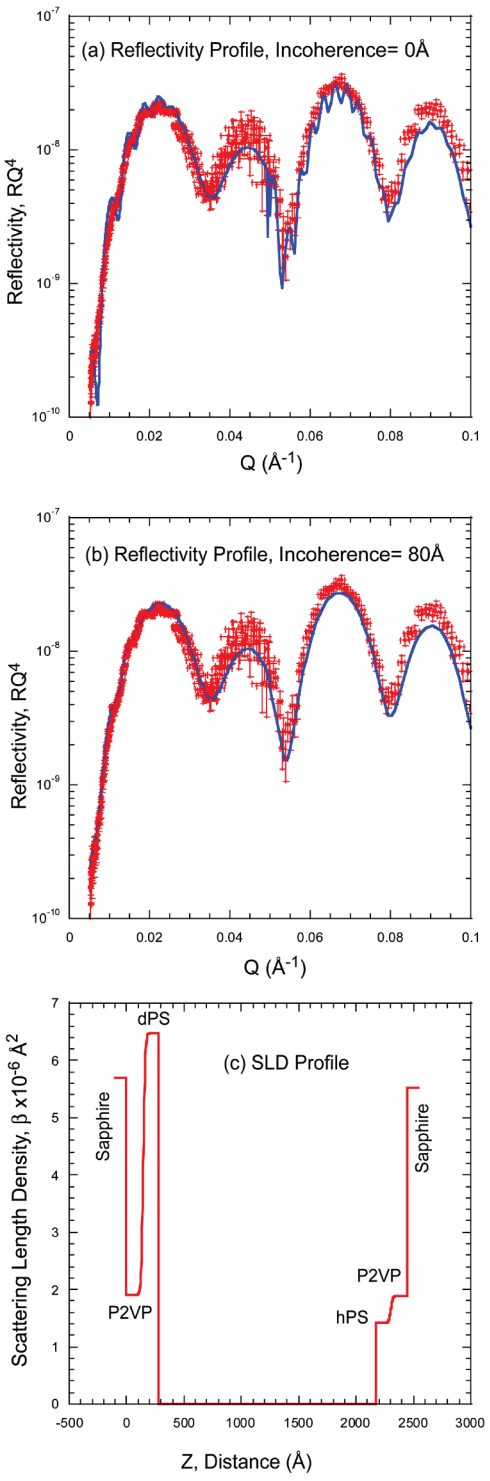

Figure 1-7 (a) Reflectivity profile for an opposing spincoated dPS–P2VP layer facing hPS-P2VP layer. The small Q interference peaks in the profile result from constructive interference between the substrates and their overall separation. The higher Q peaks are due to the polymer layers. The solid curve is a fit to the data based on (c) the SLD profile. (b) Reflectivity profile generated by the incoherent averaging of the calculated model reflectivity (c) over an 80Å Gaussian distribution of gap thicknesses.

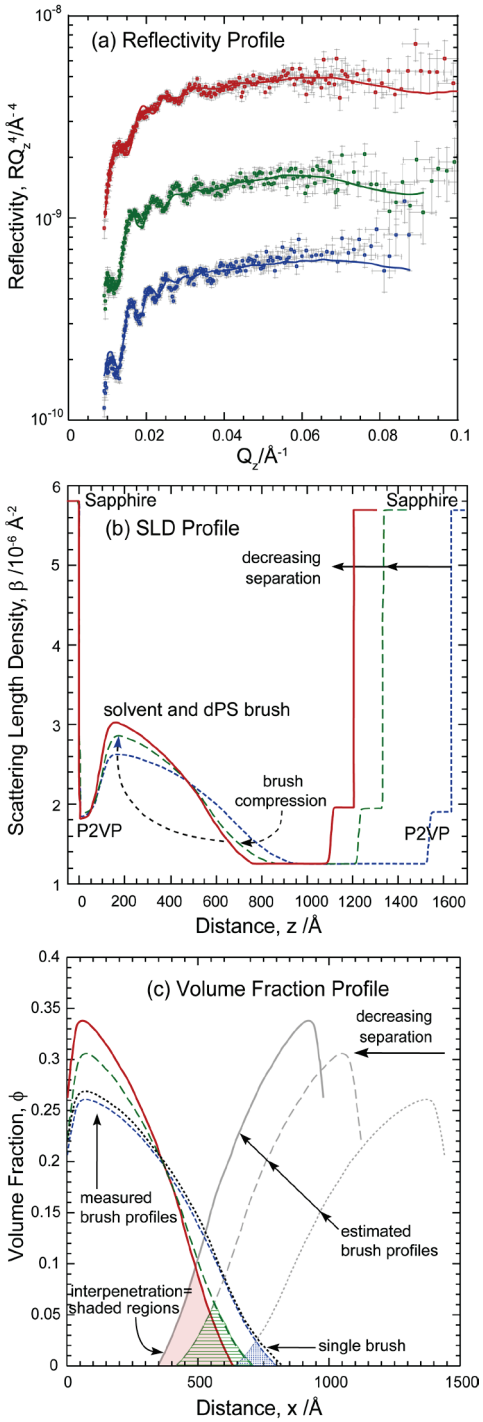

Figure 1-8 Neutron reflectivity data for three different compressions of asymmetric dPS – hPS brushes in toluene contrast matched to hPS. Solid curves are fits to the data based on the scattering length density (SLD) profiles shown in (b). Only the dPS brush is visible under these conditions (left hand side). Significant compression of the brush is found with increasing confinement. (c) Volume fraction profiles from the fits for the three compressions. A mirrored image of the dPS profile is shown (grey lines) to highlight the level of interpenetration. The mirrored profiles are in excellent agreement with the measured symmetric profiles shown in Figure 5c. For comparison, the heavy dotted line is the measured profile for an unconfined brush at a single surface.

Table 1-4 Opposing Asymmetric Polymer Brush Fitting Parameters

Solvent	dPS T (Å)		dPS SLD				
Air	120		6.4				
Toluene	h_1 (Å)	h_2 (Å)	$SLD(0)$	$SLD(h_1)$	$SLD(h_2)$	n_1	n_2
Small	430	250	3.07	2.1	1.25	1.7	1.5
Medium	430	360	2.90	2.1	1.25	1.8	1.9
Large	535	400	2.83	1.8	1.25	1.5	1.7

Solvent	$P2VP_1$ T (Å)	$P2VP_1$ SLD	$P2VP_2$ T (Å)	$P2VP_2$ SLD	S_1 SLD	S_2 SLD
Air	130	1.90	2.10	1.90	5.70	5.6
Toluene						
Small	90	1.82	100	1.95	5.80	5.70
Medium	95	1.85	105	1.95	5.80	5.70
Large	90	1.80	107	1.95	5.80	5.70

			Roughness (Å)				
Solvent	χ^2	Incoh (Å)	$P2VP_1$-dPS	hPS-$P2VP_2$	S_1-$P2VP_1$	$P2VP_2$-S_2	PS-Air
Air	2.3	65	15	15	2	2	4
Toluene							
Small	2.4	80	28	7	1	1	
Medium	2.0	80	30	5	2	2	
Large	3.4	80	30	1	3	2	

Theta Solvent

The comparison of the good vs. theta solvent qualities is particularly interesting due to the differences in frictional properties of PS brushes under these two conditions. In contrast to a good solvent where solvent-polymer intermolecular forces dominate, the solvent-polymer repulsive forces are canceled by the monomer-monomer attractive forces and the brush behaves like an ideal random coil. Experimentally, in a good solvent, PS brushes need to be compressed to ~15% of their equilibrium height before frictional forces are measured using the surface force apparatus, suggesting little interpenetration of the opposing brushes [30, 33, 34]. When a near-theta solvent of cyclohexane at 32°C was used, frictional forces were measured when the brush layer was only mildly compressed (90% of the equilibrium height). Changing the cyclohexane to a "good" solvent by increasing the temperature to 50°C does not significantly change the equilibrium extension of the brush; however, the frictional forces substantially decrease [30, 33, 34]. These findings strongly suggest that the brushes are highly interpenetrated under theta conditions and as the solvent quality increases, the brushes become less interpenetrated.

Figure 1-9c shows the resulting volume fraction profile measured for a single surface and one confinement level obtained for symmetric d-PS system in cyclohexane at 32°C for $D \approx 550$ Å. The SLD profile in 1-9b followed the same form as the symmetric brushes in good solvent. Parameters for the solvated and air fits are given in Table 1-5. Under confinement in theta solvent, the brushes compress against the anchor solvent with compression. This is surprising as much more interpenetration was expected based on friction studies. Unfortunately, only one confinement level has been achieved

due to challenges with solvating the system and alignment. Under theta solvent conditions, the surfaces must be much closer together for the brushes to touch than that of the good solvent system since the extension of the brush is much less.

Table 1-5 Opposing Symmetric Polymer Brush Fitting Parameters

Solvent	D (Å)	dPS T (Å)		dPS SLD				
Air	506	110		6.4				
		h_1 (Å)	h_2 (Å)	$SLD(0)$	$SLD(h_1)$	$SLD(h_2)$	n_1	n_2
h-Cyclohexane	550	185	250	3.40	2.00	1.75	1.5	1.75

Solvent	P2VP T (Å)	P2VP SLD	Q SLD	S SLD
Air	140	1.90	4.2	5.65
h-Cyclohexane	137	1.85	4.2	5.74

			Roughness (Å)		
Solvent	χ^2	Incoh (Å)	P2VP-PS	Q-P2VP	P2VP-S
Air	2.94	90	7	1	1
h-Cyclohexane	4.0	50	11	5	5

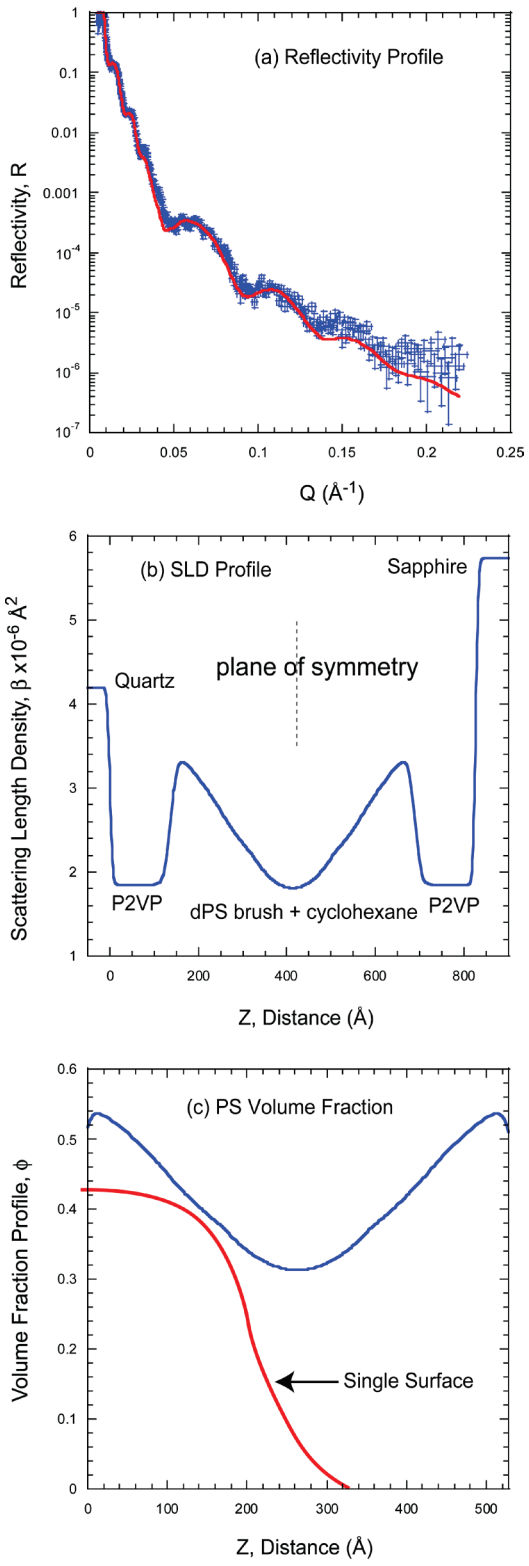

Figure 1-9 (a) Neutron reflectivity data for one gap spacing with symmetric dPS brushes in cyclohexane; a theta solvent for PS. The solid curve is a fit to the data based on SLD profile shown in (b). (c) Volume fraction profile of the confined brushes in comparison to that an unconfined brush at a single surface.

Conclusions

These direct, in-situ measurements of polymer brush density profile as a function of confinement provide an unprecedented ability to investigate the behavior of polymers in restricted geometries. Our findings demonstrate that strongly stretched brushes in good solvent conditions compact against the anchoring surface with compression rather than interpenetrate significantly under confinement and provide new insight into why such layers are so effective at reducing friction and wear. In addition, these experimental measurements point out limitations of current theoretical treatments in capturing the behavior of polymer brushes in restricted geometries. Preliminary results under theta solvent conditions demonstrate a similar behavior.

References

1. Kent, M.S., *A quantitative study of tethered chains in various solution conditions using Langmuir diblock copolymer monolayers.* Macromolecular Rapid Communications, 2000. **21**(6): p. 243-270.

2. Karim, A., Satija, S.K., Douglas, J.F., Ankner, J.F., and Fetters, L.J., *Neutron Reflectivity Study of the Density Profile of a Model End-Grafted Polymer Brush - Influence of Solvent Quality.* Physical Review Letters, 1994. **73**(25): p. 3407-3410.

3. Levicky, R., Koneripalli, N., Tirrell, M., and Satija, S.K., *Concentration profiles in densely tethered polymer brushes.* Macromolecules, 1998. **31**(11): p. 3731-3734.

4. Milner, S.T., Witten, T.A., and Cates, M.E., *Theory of the Grafted Polymer Brush.* Macromolecules, 1988. **21**(8): p. 2610-2619.

5. Field, J.B., Toprakcioglu, C., Dai, L., Hadziioannou, G., Smith, G., and Hamilton, W., *Neutron Reflectivity Study of End-Adsorbed Diblock Copolymers - Cross-over from Mushrooms to Brushes.* Journal De Physique Ii, 1992. **2**(12): p. 2221-2235.

6. Field, J.B., Toprakcioglu, C., Ball, R.C., Stanley, H.B., Dai, L., Barford, W., Penfold, J., Smith, G., and Hamilton, W., *Determination of End-Adsorbed Polymer Density Profiles by Neutron Reflectometry.* Macromolecules, 1992. **25**(1): p. 434-439.

7. Kent, M.S., Lee, L.T., Factor, B.J., Rondelez, F., and Smith, G.S., *Tethered chains in good solvent conditions: An experimental study involving Langmuir diblock copolymer monolayers.* The Journal of Chemical Physics, 1995. **103**(6): p. 2320-2342.

8. Tauton, H.J., Toprakcioglu, C., and Klein, J., *Direct measurement of the interaction between mica surfaces with adsorbed diblock copolymer in a good solvent.* Macromolecules, 1988. **32**(11): p. 3333-3338.

9. Schorr, P.A., Kwan, T.C.B., Kilbey, S.M., Shaqfeh, E.S.G., and Tirrell, M., *Shear forces between tethered polymer chains as a function of compression, sliding velocity, and solvent quality.* Macromolecules, 2003. **36**(2): p. 389-398.

10. Klein, J., Kamiyama, Y., Yoshizawa, H., Israelachvili, J.N., Fredrickson, G.H., Pincus, P., and Fetters, L.J., *Lubrication forces between surfaces bearing polymer brushes.* Macromolecules, 1993. **26**(21): p. 5552-5560.

11. Overney, R.M., Leta, D.P., Pictroski, C.F., Rafailovich, M.H., Liu, Y., Quinn, J., Sokolov, J., Eisenberg, A., and Overney, G., *Compliance Measurements of Confined Polystyrene Solutions by Atomic Force Microscopy.* Physical Review Letters, 1996. **76**(8): p. 1272-1275.

12. Kelley, T.W., Schorr, P.A., Johnson, K.D., Tirrell, M., and Frisbie, C.D., *Direct force measurements at polymer brush surfaces by atomic force microscopy.* Macromolecules, 1998. **31**(13): p. 4297-4300.

13. Szleifer, I. and Carignano, M.A., *Tethered polymer layers.* Advances in Chemical Physics, Vol Xciv, 1996. **94**: p. 165-260.

14. Halperin, A., Tirrell, M., and Lodge, T.P., *Tethered Chains in Polymer Microstructures.* Advances in Polymer Science, 1992. **100**: p. 31-71.

15. Grest, G.S., *Normal and shear forces between polymer brushes.* Polymers in Confined Environments, 1999. **138**: p. 149-183.

16. Whitmore, M.D. and Baranowski, R., *End-anchored polymers: Compression by different mechanisms and interpenetration of apposing layers.* Macromolecular Theory and Simulations, 2005. **14**(2): p. 75-95.

17. Milner, S.T., *Polymer Brushes.* Science, 1991. **251**(4996): p. 905-914.

18. Kreer, T., Binder, K., and Muser, M.H., *Friction between polymer brushes in good solvent conditions: Steady-state sliding versus transient behavior.* Langmuir, 2003. **19**(18): p. 7551-7559.

19. Klein, J., *Shear, friction, and lubrication forces between polymer-bearing surfaces.* Annual Review of Materials Science, 1996. **26**: p. 581-612.

20. Witten, T.A., Leibler, L., and Pincus, P.A., *Stress Relaxation in the Lamellar Copolymer Mesophase.* Macromolecules, 1990. **23**: p. 824-829.

21. Wijmans, C.M., Zhulina, E.B., and Fleer, G.J., *Effect of Free Polymer on the Structure of a Polymer Brush and Interaction between Two Polymer Brushes.* Macromolecules, 1994. **27**: p. 3238-3248.

22. Martin, J.I. and Wang, Z.G., *Polymer Brushes - Scaling, Compression Forces, Interbrush Penetration, and Solvent Size Effects.* Journal of Physical Chemistry, 1995. **99**(9): p. 2833-2844.

23. Neelov, I.M., Borisov, O.V., and Binder, K., *Shear deformation of two interpenetrating polymer brushes: Stochastic dynamics simulation.* Journal of Chemical Physics, 1998. **108**(16): p. 6973-6988.

24. Russell, T.P., *Methods for Characterizing Polymer Surfaces and Interfaces.* Chimia, 1990. **44**(10): p. 312-315.

25. Kuhl, T.L., Smith, G.S., Israelachvili, J.N., Majewski, J., and Hamilton, W., *Neutron confinement cell for investigating complex fluids.* Review of Scientific Instruments, 2001. **72**(3): p. 1715-1720.

26. Cosgrove, T., Zarbakhsh, A., Luckham, P.F., Hair, M.L., and Webster, J.R.P.W., *Adsorption of Polystyrene-Poly(Ethylene Oxide) Block-Copolymers on Quartz Using a Parallel-Plate Surface-Force Apparatus and Simultaneous Neutron Reflection.* Faraday Discussions, 1994(98): p. 189-201.

27. Cosgrove, T., Luckham, P.F., Richardson, R.M., Webster, J.R.P., and Zarbakhsh, A., *The Measurement of Volume Fraction Profiles for Adsorbed Polymer under Compression Using Neutron Reflectometry.* Colloids and Surfaces a-Physicochemical and Engineering Aspects, 1994. **86**: p. 103-110.

28. Hamilton, W.A., Smith, G.S., Alcantar, N.A., Majewski, J., Toomey, R.G., and Kuhl, T.L., *Determining the density profile of confined polymer brushes with neutron reflectivity.* Journal of Polymer Science Part B-Polymer Physics, 2004. **42**(17): p. 3290-3301.

29. Grest, G.S., Lacasse, M.D., and Murat, M., *Molecular-dynamics simulations of polymer surfaces and interfaces.* Mrs Bulletin, 1997. **22**(1): p. 27-31.

30. Forster, A.M., Mays, J.W., and Kilbey, S.M., *Effect of temperature on the frictional forces between polystyrene brushes.* Journal of Polymer Science Part B-Polymer Physics, 2006. **44**(4): p. 649-655.

31. Kreer, T., Muser, M.H., Binder, K., and Klein, J., *Frictional drag mechanisms between polymer-bearing surfaces.* Langmuir, 2001. **17**(25): p. 7804-7813.

32. Smith, G.S., Kuhl, T.L., Hamilton, W.A., Mulder, D., and Satija, S.K., *Neutron reflectometry studies of polymer brushes in confined geometry subject to shear.* Abstracts of Papers of the American Chemical Society, 2005. **230**: p. 459-ANYL.

33. M. Forster, S.M.K.I., *Effect of solvent quality on the friction forces between polymer brushes.* Mat. Res. Soc. Symp. Proc. 2002, 710, 179.

34. Forster, A.M., Mays, J.W., and Kilbey, S.M., *Effect of temperature on the frictional forces between polystyrene brushes.* Journal of Polymer Science Part B: Polymer Physics, 2006. **44**(4): p. 649-655.

Chapter 2: Structure of Confined Polymer Thin Films Subject to Shear

Based on Smith, G.S., Kuhl, T.L., Hamilton, W.A., Mulder, D.J., Satija, S., Structure of Confined Polymer Thin Films Subject to Shear. ***Physica B: Condensed Matter****, 2006.* ***385-386(Part 1)****: p. 700-702*

Abstract

Using neutron reflectivity and a newly developed Neutron Confinement Shear Cell (NCSC), the density distribution of opposing neutral polymer brushes confined between parallel plates in good solvent conditions were determined. With an average separation between the plates of approximately 1000 Å, the measurements show that the density profile in the overlap region between opposing polymer brushes flattens consistent with predictions from molecular dynamics simulations. A significant increase in density at the anchoring surfaces due to compression of the brush layers is observed. This compression or collapse of the brushes in restricted geometries strongly suggests that high-density brushes do not interpenetrate significantly in good solvent conditions. In addition, for the first time, the effects of an applied shear stress on the sample were measured. For neutral brushes, shear creates a totally new disentangled structure which surprisingly relaxes only after a time span of a few weeks.

Introduction

Polymer molecules at solid or fluid interfaces have an enormous spectrum of applications and functions in a wide variety of technologies. For example, they provide a mechanism to impart steric stabilization of colloidal dispersions, are used as protective coatings (including mechanical protection of solids against friction and wear), and are used to modulate dispersion properties (such as rheology) under a variety of processing

conditions [1] . They can be designed to either promote adhesion (e.g. epoxies and glues) or they can be used to prevent sticking (such as Teflon-coated metal surfaces). In the same manner, proteins, which are natural biopolymers, govern the interactions between and functions of biological cell surfaces.

Knowledge of the conformations that adsorbed or terminally anchored chain molecules adopt when subjected to confinement and solvent flow is essential for predicting the interaction forces, and tribological, and rheological properties in thin-film technologies [2]. Theoretical [2] and modeling [3-5] investigations have been performed on polymers chemically or physically tethered to surfaces.

When densely packed polymers attached to a substrate are placed in a good solvent (for the unbound end of the polymer), the polymer free-energy consists of a competition between the osmotic forces which want the chains to dissolve in solution and the energy cost of stretching the coiled chain. The resulting carpet-like molecular structure is referred as a polymer brush. One of the characteristic properties calculated for these systems is the polymer segment density profile normal to the surface.

Experimental

High-density polymer brushes were formed by spin coating 50:50 polystyrene-poly-2-vinlypyridine diblocks (PS-P2VP MW=122 k, polydispersity=1.1, fraction P2VP=0.51) [6, 7]. The P2VP portion of the diblock is hydrogenated while the PS portion can be either hydrogenated or deuterated to take advantage of contrast labeling. Static measurements were made with hydrogenated PS-P2VP layers. Static and shear measurements were made with deuterated PS-P2VP layers. Uniform polymer thin-films

were prepared by spin coating [6, 7] at 2000 rpm for 30 s on dry, ultra-clean sapphire substrates in a clean room environment. The sapphire substrates were precleaned in acetone, isopropanol, dried, and then cleaned for 10–20 min in 70:30 sulfuric acid:hydrogen peroxide at 100 °C. Afterwards, the substrates were cooled to less than 50 °C prior to rinsing with copious deionized water (18 MΩ cm) and dried using clean nitrogen. The spin coating solution was 6.0 mg/ml PS-P2VP in toluene. The polymer was dissolved in solution with continuous stirring and prepared at least 24 h in advance. Just prior to use, the solution was filtered a minimum of 3 times through 0.45 μm PTFE filters. The spin-coated polymer layers prepared in this manner were about 200 Å thick as determined by ellipsometry and only films with zero or few holes were used. After spin coating, the polymer thin-films were annealed under vacuum at 180 °C for 24 h. The substrates were then cooled to room temperature before removal from the vacuum oven. The glass transition temperature for both polymers is just over 100 °C [8]. P2VP prefers to wet the sapphire (oxide) surface [9] while PS segregates to the air interface. After annealing, an equilibrium alignment of lamellae parallel to the substrate occurs due to preferential surface wetting and the incompatibility of the PS and P2VP blocks.

Two substrates were coated as described above and then placed in contact. The substrates were then put into the confinement cell [10] shown schematically in Figure 2-1. Good solvent for the PS segment (deuterated toluene) was wicked into the space between the coated blocks and neutron reflectivity measurements were performed [11] on the NG-7 reflectometer at the NIST Center for Neutron Research and the SPEAR reflectometer at LANSCE.

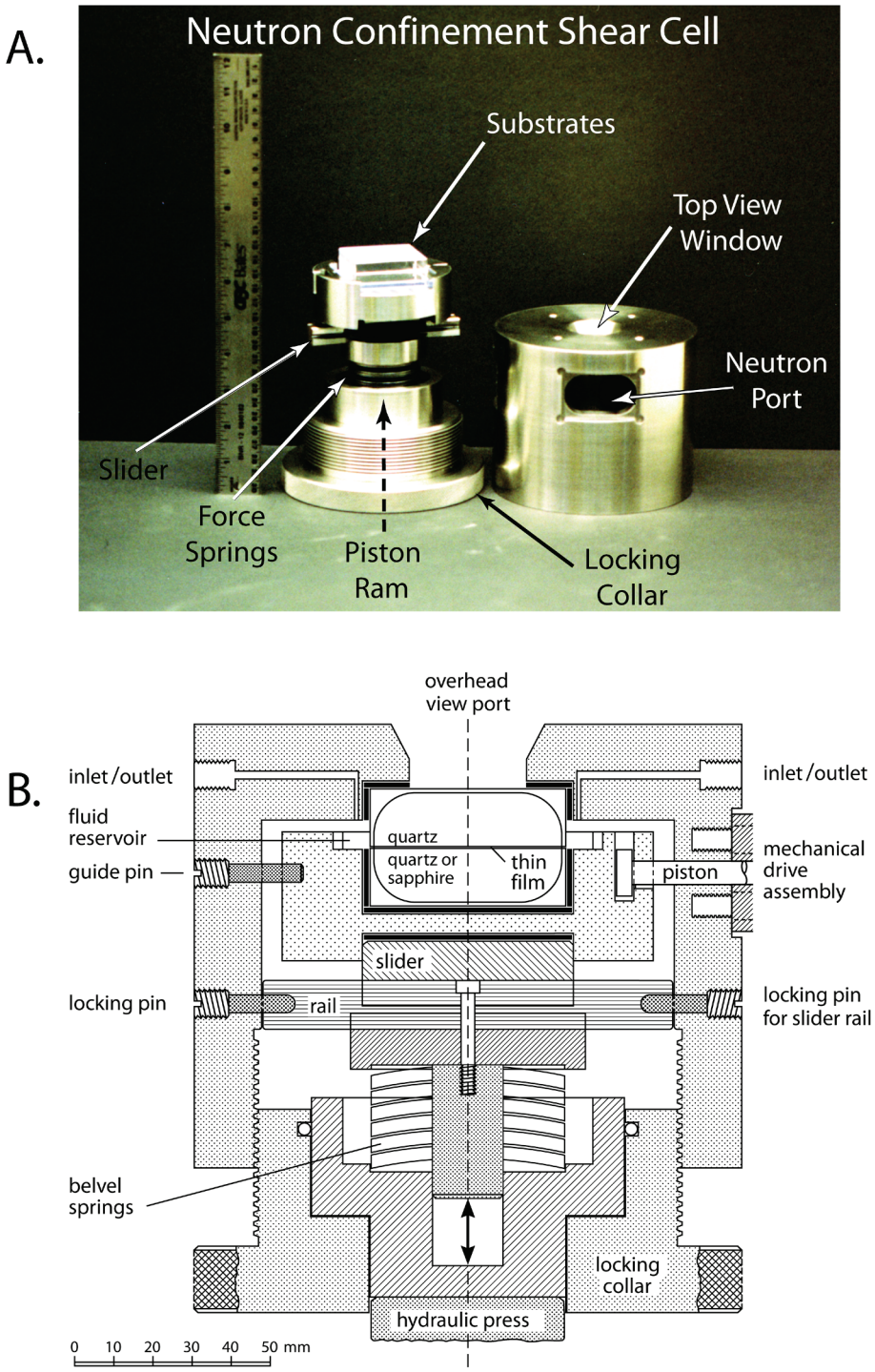

Figure 2-1 (A) Photograph of the neutron confinement cell NCSC with the outer steel housing removed. A 12 in. ruler on the left-hand side gives an idea of the size of the apparatus. (B) Cross section of the NCSC. The neutron beam passes perpendicular to the view shown. The apparatus is constructed with 304 and 316 stainless steel and all inlets and outlets are sealed by Teflon o-rings or gaskets. A hydraulic ram can be used to apply high loads, which are calibrated by measuring the compression of Belleville washers of variable spring constant. The upper quartz substrate mounts into the top of the outer housing. The lower sapphire quartz substrate mounts on a mechanical slider and can be translated sheared relative to the upper surface using a mechanical motor drive assembly.

Results and Discussion

A typical measurement for the solvated brushes with a fit to the data is shown in Figure 2-2. The resulting PS volume fraction profiles for brushes at plate separations of 1175 and 850 Å are plotted in Figure 2-3.

An identical form for the scattering length density (SLD) profile was utilized for both the 850 and the 1175 Å gap consisting of a parabola and a flat gap to describe the PS block SLD [11]. The SLD of the parabola used to model the PS brushes and the gap SLD were allowed to vary in order to accommodate the squeezing out of d-Toluene from between the substrates and changes in the density profile of the more confined PS brushes. A comparison of the resulting volume fraction profiles for the two different confinement levels are provided in Figure 2-3. A constant amount (±2%) of PS was obtained as expected from conservation of mass. The ability of our simple model to fit both sets of data suggests that the model represents the physical system reasonably well.

For shear measurements, the NCSC (Figure 2-1) has a linear ball slide attached to one of the substrates. The ball slide is attached to a stepper motor through a rotary-to-linear gear box. When the movable substrate is driven parallel to the fixed surface at a constant velocity, the fluid between the surfaces is sheared at a constant rate.

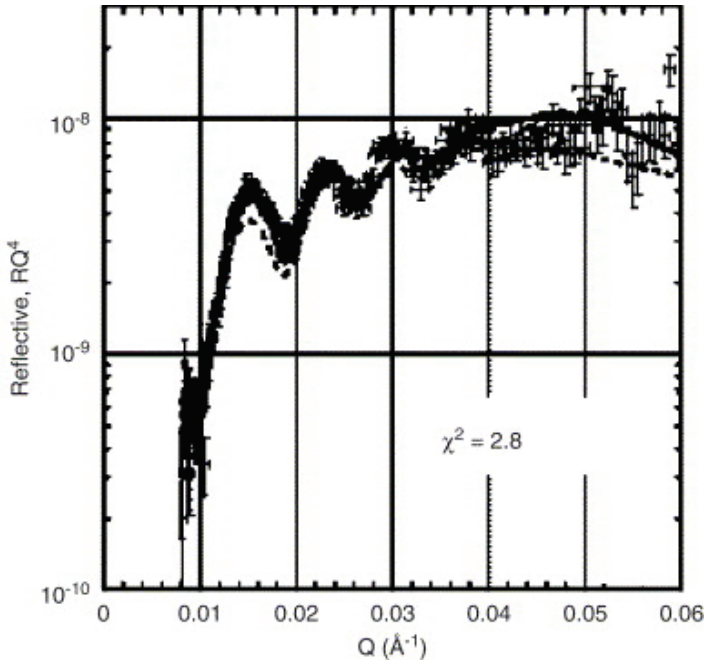

Figure 2-2 Reflectivity profile for a plate separation of ~850 Å. The solid curve is a fit to the data with a parabola plus a flat region representing the PS. The dashed curve is a fit (χ^2=4.3) to the data based on a single flat density profile for the PS.

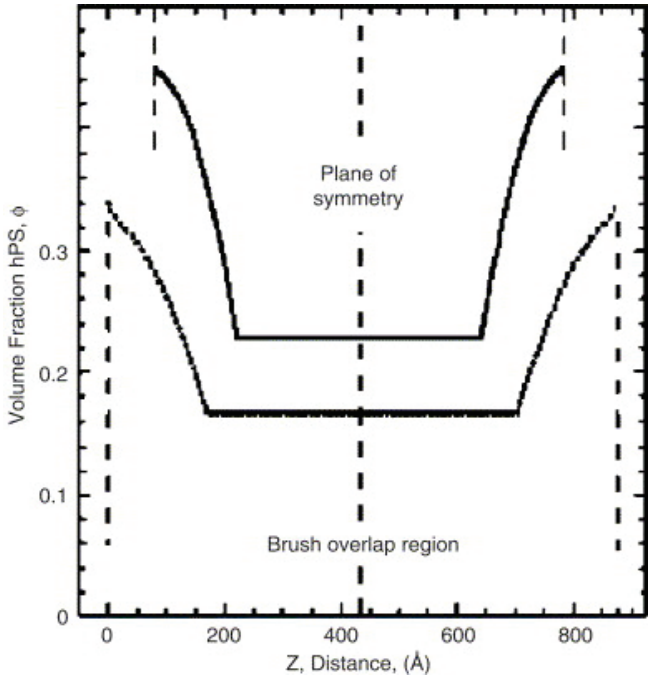

Figure 2-3 Volume fraction profiles of the PS portion of the brush for the 1175 Å (lower curve) and 850 Å (upper curve) inter-substrate separation. There is significant confinement of the opposing polymer brush layers causing the density of overlap region to increase and flatten[3-5]. At the greater level of confinement, the density of PS portion of the diblock further increases at the P2VP substrate surface.

For the shear runs, a diblock copolymer where the PS block was deuterated was solvated with protonated toluene. The samples were prepared as describes above for the static measurements. Before shear, static reflectivity measurements were run to determine the initial structure and ensure good alignment of the surfaces. A shear forced was then applied to the film. For the first measurement, we drove the two surfaces past each other over a distance of 5 mm and a rate of roughly 1 mm/s. The reflectivity measurements were then repeated as a function of time with the plates stationary (Figure 2-4). Surprizingly, there was a large change in the reflectivity curve after the motion. The change has a very long relaxation time of several days. Measurements were repeated periodically over a few days. Only after several days did the curve resemble the unsheared version. These are the first measurements on a molecular length scale showing structural changes of a polymer as a function of shear in a good solvent.

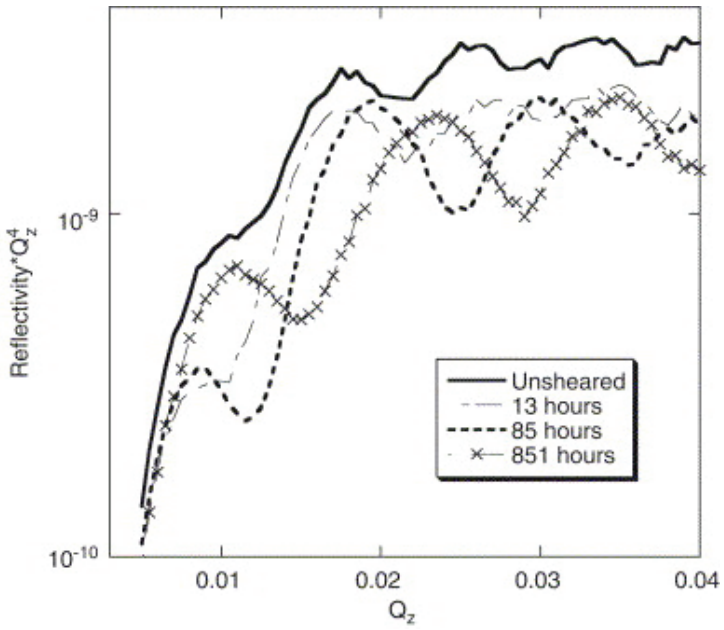

Figure 2-4 Neutron reflectivity measurements of shear/confined PS-PVP diblock. The data was first measured without shearing in a good solvent. Then the sample was sheared and the measurements repeated. Several days after the shear was applied, the profiles returned to the original data.

Qualitatively, the data in Figure 2-4 show a shift of the interference fringes to larger separations of Q_z in the post-shearing data versus the unsheared data. This implies that the gap thickness has decreased. Perhaps more interesting is that the post-shearing data not only shows this shift, but also has more visible fringes demonstrating that the two surfaces became better aligned after shearing [11].

Conclusions

In conclusion, neutron reflectivity can be utilized to determine the density distribution of opposing polymer brush layers as a function of confinement. The resultant volume fraction profiles are consistent with predictions from molecular dynamics simulations and mean field theory showing a flattening in the overlap region. However, a significant increase in concentration at the di-block interface was also evident, which had not been previously suggested, and indicates that compression of the brushes is more dominant than interdigitation. In addition, the reflectivity from a polymer in confinement and subject to shear has been measured.

References

1. Dunn, A.S., *Polymeric stabilization of colloidal dispersions. By D. H. Napper, Academic Press, London, 1984. pp. xviii + 428, price £39.50, $65.00. ISBN 0-12-513980-2.* British Polymer Journal, 1986. **18**(4): p. 278-278.

2. Milner, S.T., *Polymer Brushes.* Science, 1991. **251**(4996): p. 905-914.

3. Grest, G.S., *Normal and shear forces between polymer brushes.* Polymers in Confined Environments, 1999. **138**: p. 149-183.

4. Ruckenstein, E. and Li, B.Q., *Steric interactions between two grafted polymer brushes.* Journal of Chemical Physics, 1997. **107**(3): p. 932-942.

5. Murat, M. and Grest, G.S., *Interaction between grafted polymeric brushes: A molecular-dynamics study.* Physical Review Letters, 1989. **63**(10): p. 1074-1077.

6. Levicky, R., Koneripalli, N., Tirrell, M., and Satija, S.K., *Concentration profiles in densely tethered polymer brushes.* Macromolecules, 1998. **31**(11): p. 3731-3734.

7. Levicky, R., *Polymer Brushes and Mesogels in selectively swollen block copolymer films, Dissertation.* December 1996.

8. Dechant, J., *Polymer handbook. 3rd edition. J. BRANDRUP and E. H. IMMERGUT (editors). ISBN 0-471-81244-7. New York/Chichester/Brisbane/Toronto/Singapore: John Wiley & Sons 1989. Cloth bond, ca. 1850 pages, £ 115.00, $175.00.* Acta Polymerica, 1990. **41**(6): p. 361-362.

9. Ruths, M., Johannsmann, D., RÃ¼he, J., and Knoll, W., *Repulsive forces and relaxation on compression of entangled, polydisperse polystyrene brushes.* Macromolecules, 2000. **33**(10): p. 3860-3870.

10. Kuhl, T.L., Smith, G.S., Israelachvili, J.N., Majewski, J., and Hamilton, W., *Neutron confinement cell for investigating complex fluids.* Review of Scientific Instruments, 2001. **72**(3): p. 1715-1720.

11. Hamilton, W.A., Smith, G.S., Alcantar, N.A., Majewski, J., Toomey, R.G., and Kuhl, T.L., *Determining the density profile of confined polymer brushes with neutron reflectivity.* Journal of Polymer Science Part B-Polymer Physics, 2004. **42**(17): p. 3290-3301.

Chapter 3: Structural Determination of High Density, ATRP Grown Polystyrene Brushes by Neutron Reflectivity

Based on Ell, J.R., Mulder, D. J., Faller, R., Patten, T.E., Kuhl, T.L., Structural Determination of High Density, ATRP Grown Polystyrene Brushes by Neutron Reflectivity. ***Macromolecules,*** *2009* ***42 (24)****, 9523-9527*

Abstract

The development of well controlled synthetic schemes for growing polymer brushes directly from surfaces has recently enabled very high polymer grafting densities to be explored. For these studies, polystyrene brushes were prepared by atom transfer radical polymerization (ATRP) at a high grafting density of 0.44 chains/nm^2. Molecular weights from 15 to 45k were studies. The dry film thickness scaled linearly with chain molecular weight. Under good solvent conditions, strongly stretched brushes of moderate molecular weight were found to maintain a parabolic density distribution consistent with theoretical predictions. Anomalous behavior was observed for higher molecular weights suggesting that entanglements are much more pronounced in "grafted from" systems.

Introduction

Grafted polymer thin films and brushes are frequently formed by physisorption, chemisorption of block copolymers, or binding of end-functionalized polymer chains to surfaces [1]. These materials are a practical way to modify the mechanical or chemical properties of surfaces. Their structure, once solvated, has been studied extensively allowing an in-depth understanding of their properties and use as lubrication, adhesion, and surface compatibilization modifiers in a wide array of applications. Brush structure and hence properties depend strongly on their grafting density, σ, at the anchor surface. For example, at low grafting densities ($\sigma^* < 1$, where $\sigma^* = \sigma\pi R_g^2$ is the reduced surface density and R_g is the radius of gyration) the chains are sufficiently far apart that they can adopt coiled conformations, and are in the so-called "mushroom regime." In good solvent conditions, the height of low density brush scales approximately as the unperturbed coil radius, $N^{3/5}$. The semi-dilute brush regime occurs at somewhat higher grafting densities ($\sigma^* \geq 1$). These types of films have been the most studied. In the semi-dilute regime, the brush height scales as $N\sigma^{1/3}$. The higher exponent for N relative to the mushroom regime films indicates that the chains are stretched due to interchain repulsive interactions resulting from their closer packing. The third structural regime ($\sigma^* >> 1$) is the "concentrated brush" or strongly stretched regime. At the extreme end of grafting levels, the equilibrium layer thickness approaches the length of a completely stretched polymer chain [2]. It is known that semidilute brush theory breaks down in the concentrated brush regime, as the scaling exponent apparently increases with increasing graft density.

Experimental studies at the very high grafting density regime are rare due to the challenges associated with forming such layers. "Grafting from" approaches provide access to this regime by polymerizing monomers directly onto a surface from solution. Typically, a monolayer of polymerization initiator is attached to a surface and polymerization occurs via monomer diffusion to the active sites of the growing polymer chains. This growth process can be contrasted to "grafting to" methods, in which the layer thickness must increase by diffusion of a polymer chain through the brush layer to the substrate surface. While several conventional and living ionic polymerization methods have been applied to the synthesis of polymer films, a recent breakthrough in the preparation of highly concentrated grafting regimes followed the development of living radical polymerization (LRP) [3-8]. LRP methods have allowed for the facile preparation of grafted polymer chains with different compositions and permitted access to a large range of grafting densities using one synthetic method [2, 9-30].

Recent studies of very concentrated grafted chains have shown that their properties can differ significantly from those of semidilute brushes [13, 31]. For example, poly(methyl methacrylate) brushes formed using ATRP have been found to have much better lubrication properties compared to brushes formed using "grafting to" methods, including lower friction coefficients and increased wear resistance [32]. These enhanced properties were attributed to the extremely high grafting density and covalent anchoring of the polymer layer. Fukuda and coworkers have demonstrated facile control of the grafting density, $0.07 < \sigma$ (chains/nm^2) < 0.7, and in a recent neutron surface reflectivity study, Devaux, *et al.* reported that ultra-high density brushes polystyrene (PS) brushes grafted from Si wafers using TEMPO mediated polymerization with $\sigma = 1.1$

chains/nm^2 had very low swelling behavior in a good solvent [13]. Other affected properties include lower mechanical compressibility and higher glass transition temperatures of concentrated brushes as compared to semidilute brushes [31].

Most literature work on using living radical polymerizations to prepare grafted polymer films has employed ellipsometry for structural characterization. Here, ATRP grown PS films were characterized using neutron reflectometry which provides higher resolution information of the film's thickness, density profile, roughness, and uniformity. Because neutrons interact with the nuclei of atoms in the film rather than electrons, radiation damage is negligible and the contrast can be enhanced by using different isotopes (i.e., H and D) while the chemistry of the materials remains unaltered. Consequently, neutron reflectometry has the potential to reveal significant relationships between the structure of the brushes and their methods of preparation. In this study a series of PS grafted silicon surfaces with varying molecular weights were prepared using identical reaction conditions, varying only the residence time of the substrate in the reaction vessel. Molecular weight, grafting density, thickness, and structure of the polystyrene films were characterized by neutron reflectivity as dry films and solvated brushes in the good solvent, toluene.

Experimental

Materials

All chemicals were purchased from Aldrich and Acros and used without further purification unless otherwise reported. Styrene was stirred over CaH_2 and distilled under reduced pressure to remove the inhibitor and stored at 4°C and under N_2. Copper

Bromide (CuBr) was stirred in glacial acetic acid for 24h washed with copious amounts of ethanol, filtered and stored under N_2 until needed. Karstedt's catalyst solution was prepared as reported by Hitchcock and Lappert [33].

Initiator Synthesis

Synthesis was carried out by John R. Ell, PhD Chemistry, University of California, Davis, 2008

Allyl-11-undecanebromoisobutyrate was synthesized following established procedures [34]. In a modification to literature procedure [34], 10-undecenyl 2-bromoisobutyrate (5.00 g, 12.2 mmol) and a stir bar were evacuated and back-filled with N_2 (3x) in an oven dried 50 mL thick walled Schlenk flask. Karstedt's catalyst (83 µL, 0.375 M) was added, and the flask was cooled to 0ºC [34, 35]. Trichlorosilane (TCS) (4.75 mL, 47 mmol) was injected into the reaction flask under a stream of N_2. The flask was then sealed with a threaded PTFE stopper with a Viton o-ring, and the solution was allowed to warm to room temperature and later heated for 5 h at 40 ºC. The solution was cooled , immediately transferred to a round bottom flask and vacuum distilled at 20 mTorr @ 100°C, which yielded (3.73 g, 74 %) of a clear liquid. ^{1}H NMR: (600 MHz, $CDCl_3$) δ (ppm) 1.25-1.40 (16H, broad), 1.55 (2H, m), 1.65 (2H, m), 1.95 (6H, s), 4.2 (2H, t). ^{13}C NMR: (150 MHz, $CDCl_3$) δ (ppm) 22, 25, 26, 28.5, 29.2, 29.3, 29.5, 29.63, 29.66, 30.9, 32.2, 55.8, 66.5, 171.4. FTIR (neat): ν (cm^{-1}) 2987, 2932, 2879, 1740.

Preparation of ATRP Grafted PS Chains

PS brushes were prepared using a modified literature procedure [36]. Single crystal silicon and quartz substrates (2" diameter 1/2" thick) were cleaned in acetone, isopropanol, and copious amounts of water, dried and then exposed to UV / ozone for 20

min prior to initiator self-assembly from 1-2 mM [11-(2-bromo-2-methyl) propionyloxy) undecyl trichlorosilane in toluene. After drying the measured water contact angle of the initiator film was 80.1±0.9°.

A custom reaction flask made to accommodate the large substrates was charged with CuBr (124 mg, 0.846 mmol), $CuBr_2$(10 mg, 0.0432 mmol), and the initiator functionalized surface and then vacuum / backfilled 3 times. In a separate Schlenk flask that was also vacuum / backfilled 3 times, the styrene (10 mL, 86.4 mmol), toluene (5 mL), and ethyl 2-bromoisobutyrate (13 μL, 0.09 mmol) as the sacrificial initiator were added. The solution was degassed using three freeze / pump / thaw cycles in liquid N_2. This solution was then transferred via cannula into the reaction flask followed by injection of N,N,N',N',N"-pentamethyldiethylenetriamine (PMDETA) (189 μL, 0.907 mmol) ligand. The flask was heated at 90°C for a specified amount of time. The time to achieve a given molecular weight was estimated using calibration reaction. An identical reaction using the conditions described above was performed in which samples were taken every hour via a purged syringe. The monomer conversion was determined using GC, and the molecular weights (M_n) were determined using GPC). The polymerization was terminated by removing the heat source, exposing the reaction to air and diluting the reaction solution with copious amounts of tetrahydrofuran (THF). The supernatants (in all cases PDI < 1.10) were retained and the free polymer chains were analyzed using GPC. The film coated substrate was then immersed three times in fresh batches of hot toluene (200mL) for 1h to remove any residual polymer. Samples were stored in airtight containers until use.

Neutron Reflectivity Measurements

Specular reflectivity measured as a function of momentum transfer, $Q_Z = (4\pi \sin\theta)/\lambda$, provides information on the in-plane average coherent scattering length density (SLD) profile. Neutron reflectivity measurements were performed on both the time-of-flight SPEAR reflectometer at the Manuel Lujan Neutron Scattering Center, Los Alamos National Laboratory and the NG7 horizontal reflectometer at the Center for Neutron Research, National Institute of Standards and Technology, Gaithersburg. At SPEAR, the range of neutron wavelengths was λ = 2-16Å with a Q_Z range from 0.008 to about 0.30Å^{-1}. The neutron wavelength at NG7 was 4.760 Å with a Q_Z range of 0.007 to 0.15 Å^{-1}. The error bars on the data represent the statistical errors in the measurements (standard deviation, δR) where the uncertainty in the Q_Z resolution, ΔQ_Z / Q_Z, was nearly constant over this scattering vector range with a value of ~3%.

Results and Discussion

Dry Films

Neutron reflectivity data was collected for several substrates with different grafted PS molecular weights. The data were fit with nonlinear least-squares regression using the MOTOFIT reflectivity analysis package [37]. Figure 3-1 shows the reflectivity data and scattering length density (SLD) profile for dry PS films in air with M_n = 20k and 44k. The SLD model consisted of several layers: silicon substrate, 15-25Å native oxide, 15-20Å initiator with a SLD of 0.4x10^{-6}Å^{-2}, polystyrene, and air. The SLD of the polymer layer converged to 1.45x10^{-6}Å^{-2} compared to the expected value of 1.42x10^{-6}Å^{-2} for bulk PS, thus lending credence to the quality of the polymerization. Atomic force microscopy (AFM) showed uniform topography of the films in air with an rms roughness of 0.5 nm.

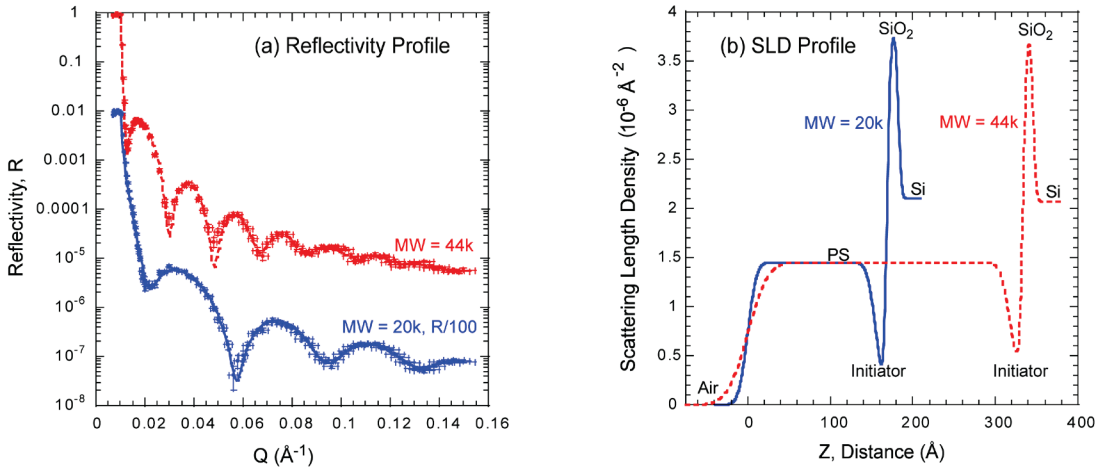

Figure 3-1(a) Reflectivity profile for two different MW PS films. Line fits to the data are based on the SLD profiles shown in (b).

Figure 3-2 shows the dry thickness, t, of the PS layers in air versus molecular weight of the free polymer from the corresponding experiment. The PS film thickness scales linearly with molecular weight demonstrating that the initiator layer and reaction conditions reproducibly initiate chain growth with the same grafting density and strongly suggests that the molecular weight of the grafted chains correlates well to that found for sacrificial initiator chains growing in solution [38]. The grafting density was calculated by fitting the equation $t = \left(\frac{\sigma}{\rho N_A}\right) M_n$ to the results in Figure 3-2. Using a bulk PS density [39] of ρ = 1.05 g/cm^3, the average grafting density was calculated to be 0.44 chains/nm^2. The cross sectional area of a single polystyrene chain in the crystalline state is 0.7 nm^2 [40], which yields a theoretical maximum grafting density of 1.4 chains/nm^2.

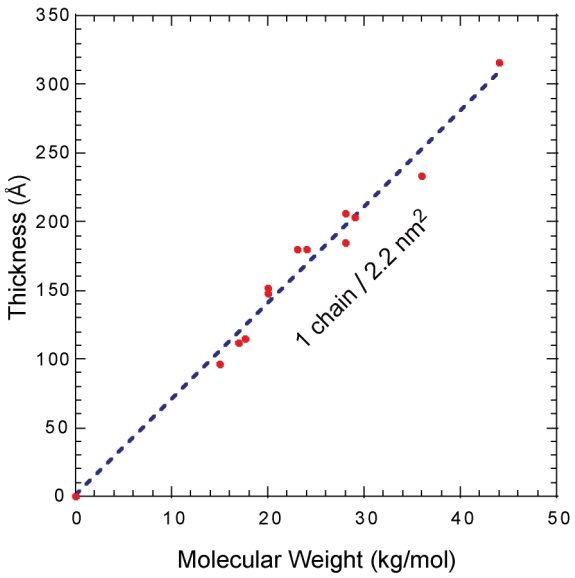

Figure 3-2 Thickness of dry PS films as a function of MW

Solvated Films

For uniformly grafted polymer brushes in good solvent, both theory and simulations predict a parabolic density profile away from the surface followed by a long decaying tail [41-45]. Figure 3-3 shows the reflectivity data (a) and best fit based on the SLD profile (b) for M_n = 15k and 23k layers in deuterated toluene (SLD=5.66x10^{-6}Å^{-2}). Deuterated toluene is a good solvent for polystyrene and maintains high neutron contrast to the grafted chains. The substrate was placed in a MACOR (machinable glass-ceramic) solid-liquid cell (Figure 3-4 and Figure 3-5). MACOR is used to absorb neutrons that have passed through the substrate, polymer, and solvent to decrease unwanted scattering. After the data were acquired, the films were allowed to dry and reflectivity measurements were performed again. The profile returned to the original pre-solvated state confirming that there were no changes to the film. The solvated data was analyzed using the MIRROR fitting program using least-squares regression [46]. The region extending from

the initiator was modeled with an additional layer to account for a possible depletion layer at the anchor surface followed by a power law profile for the brush with the end smeared by an error function representing the decaying tail.

To obtain the polymer brush density distribution, the SLD profile was converted to a volume fraction profile of PS extending from the initiator using $SLD_{fitted} = \phi_{PS}(SLD_{PS}) + (1-\phi_{PS})SLD_{toluene}$. To compare with theoretical predictions, the main body of the volume fraction profiles was fitted to a power law: $\phi(z) = \phi_0\left(1-\left(\frac{z}{h_0}\right)^n\right)$, where ϕ_0 is the volume fraction of the brush at the interface and h_0 is a measure of the brush extension. An important check of the physical correctness of the model fit was verified by conservation of mass where the amount of polymer in the solvated case matched to ±5% that found in the dry case. The volume fraction profiles and fitted power laws for M_n = 15k, 17k, 20k, and 23k are shown in Figure 3-3 and summarized in Table 3-1.

Table 3-1

$M_n \cdot 10^{-3}$ (g/mol)	N	PDI	h_{dry} (Å)	σ (chains/nm^2)	ϕ_0	h_0(Å)	n
15	144	1.08	96	0.40	0.68	174	2.50
17	163	1.06	112	0.42	0.70	216	1.95
20	192	1.05	152	0.48	0.78	277	2.15
23	221	1.05	180	0.49	0.85	261	2.30

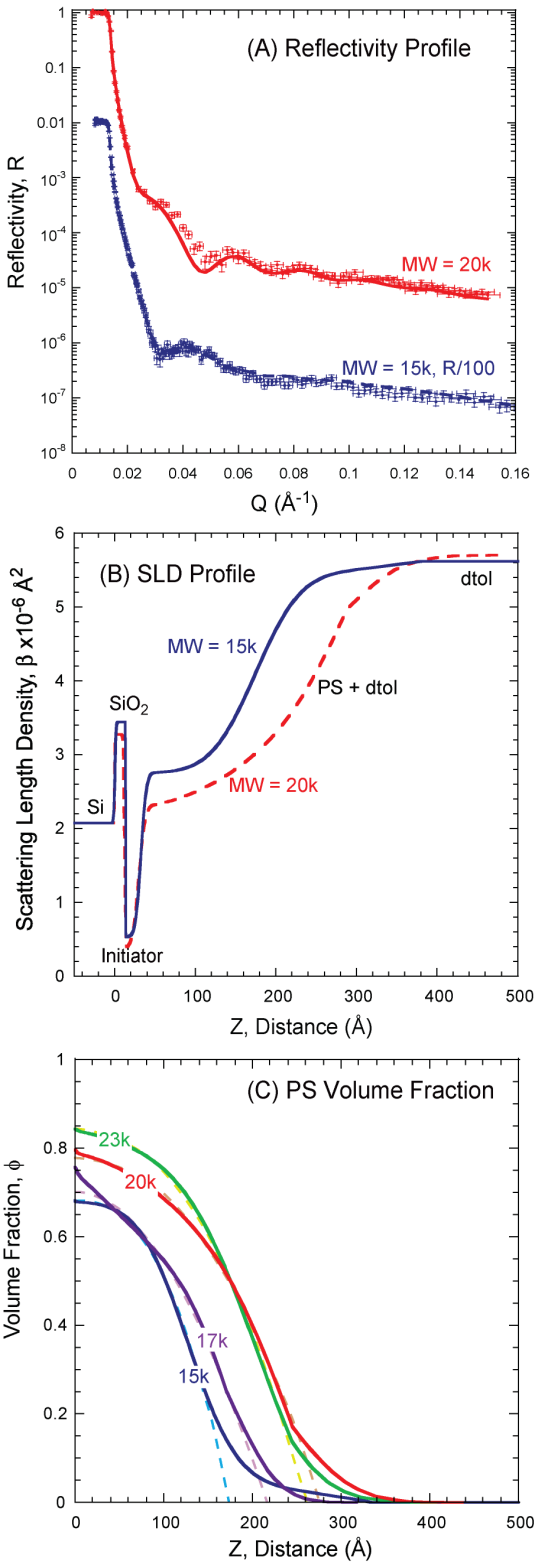

Figure 3-3 (a) Reflectivity profile for 15k and 20k PS in d-toluene. Solid and dashed curve are fits to the data based on the SLD profiles shown in (b). (c) Volume fraction profiles of PS with power law fits (dashed).

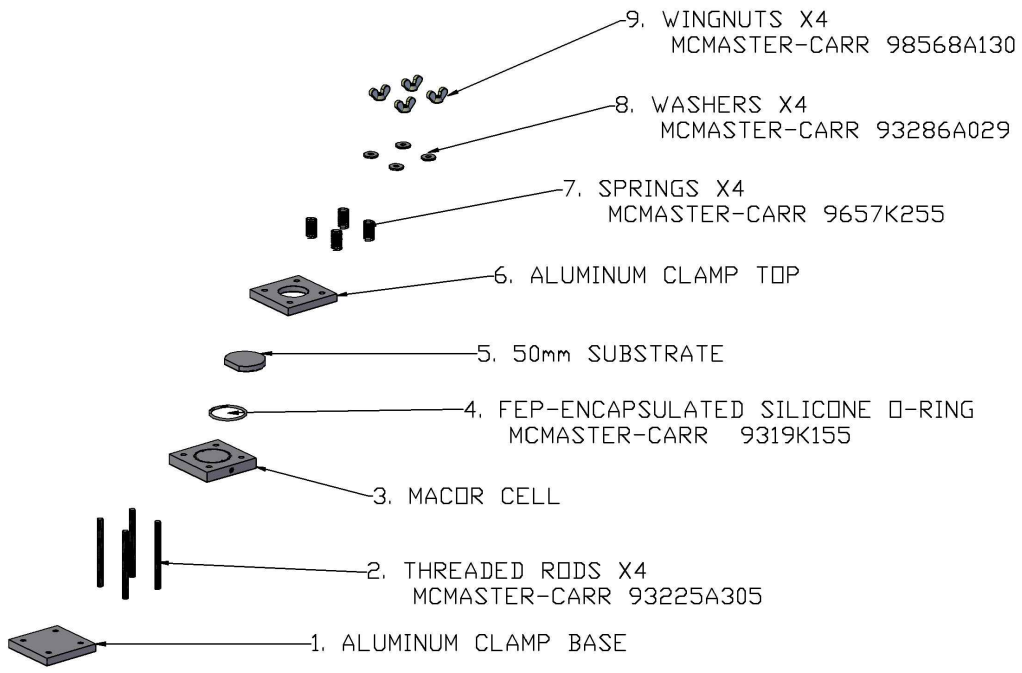

Figure 3-4 Exploded view of MACOR solid-liquid interface cell.

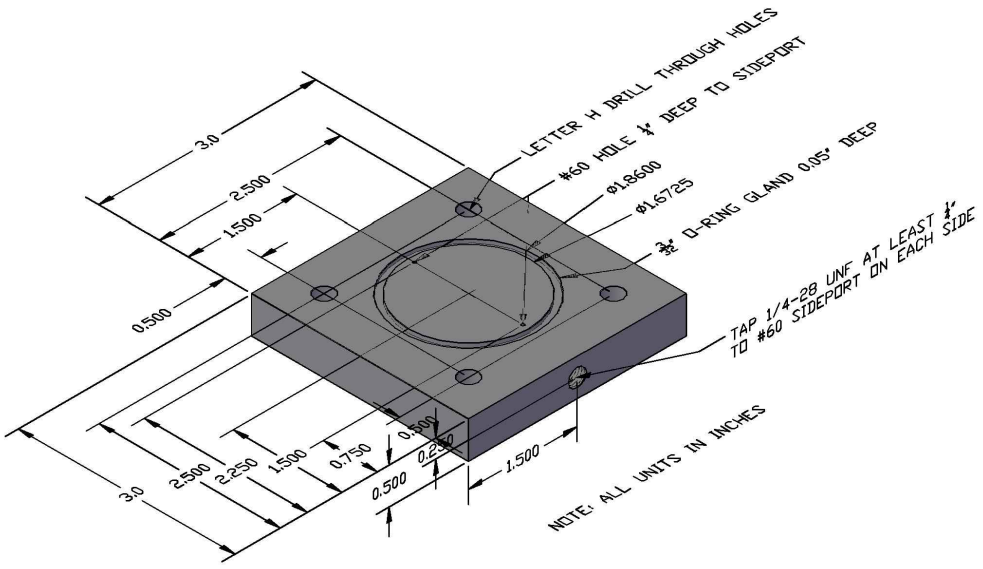

Figure 3-5 Diagram of MACOR cell, Part 3 of Figure 3-4.

The profiles of the solvated brushes (Figure 3-3c) maintain a parabolic density profile (n=2.2 ± 0.3) away from the surface followed by a smooth exponential tail. Qualitatively, this is in excellent agreement to previous neutron reflectivity work by Kent *et al.* [47], for PS at a much lower grafting density, $\sigma < 0.05$ chains/nm^2 and $2 < \sigma^* < 12$, compared to these ATRP grown samples where $\sigma = 0.44$ chains/nm^2 and $18 < \sigma^* < 30$. At lower grafting densities a depletion layer has been observed at the grafting surface, while at higher grafting densities small-angle neutron scattering work reveals no depletion layer with a parabolic profile and exponential tail [47]. The effect of a decreased depletion layer with increasing grafting density has also been observed in Monte Carlo simulations [48]. In the experiments here, no depletion layer was required to model the reflectivity data at these very high grafting densities.

Comparing all profiles (Figure 3-3c), the volume fraction at the surface increases with molecular weight. Simulations by Baranowki and Whitmore have shown the dependence of the maximum volume fraction should have a weak dependence on N and a much stronger dependence on σ scaling as $\phi_0 \propto N^{0.10}\sigma^{0.68}$ [49]. The limited data range precludes a stringent testing of this dependence, however a slightly stronger scaling with N is observed. For example, both M_n = 20k and 23k have nearly identical thicknesses and tail profiles. The increase in chain length is manifested in the increase in ϕ_0 from 0.78 to 0.85.

Although higher M_n systems were studied including M_n = 29k (Figure 3-6), monotonic density profiles were not obtained suggesting that the polymerization off the substrate was less homogeneous with time or entanglements in "grafted from" systems

are much more prevalent in surface polymerized brushes. To distinguish between these possibilities we first consider the homogeneity of the reaction. In all cases, the reaction conditions for all samples were the same, only the reaction time was varied. The measured polydispersity was also similar across all samples. There was no evidence in the GPC profile that suggested early termination or higher molecular weight coupling e.g. tail or shoulder. The percent conversion was kept between 20-60% to limit termination reactions and to retain chain-end functionality [50]. Moreover, the slightly larger polydispersity obtained from solution GPC measurements for the 15k chains is consistent with the greater exponentially decaying tail shown in the SLD profile, indicating that the analysis of sacrificial chains in the supernatant is a reliable measure of the surface grafted polymer chains. Together, these findings suggest that variations in the polymer layer structure are not due to changes in reaction kinetics. On the other hand, the entanglement molecular weight for PS is about 18k [51]. The non-montonic density distributions in the higher M_n chains are consistent with small regions of higher density within the brush layer. Such regions could result from chain "knots" or entanglements. As the reptation time for end grafted chains to detangle is very long, the observed deviations in the density distribution profiles could result from enhanced entanglements resulting in a lower brush extension with higher M_n systems. Taken together, these results suggest that "grafted from" systems may be much more entangled due to polymerization from the substrate.

Although modeling the reflectivity data for the high M_n brushes proved challenging, the solvated equilibrium brush height, h^*, could be estimated from the positions of the reflectivity data minima. Figure 3-7 shows the brush height plotted as a function of $N\sigma^{1/3}$ following the self consistent mean field (SCF) theory by Milner *et. al.*

[41] $h^* = \left(12/\pi^2\right)^{1/3} N\sigma^{1/3} \left(w/v\right)^{1/3}$ where w is the excluded volume parameter and $v = 3/b^2$ can be found from the statistical segment length, b=7.6 Å [52]. Literature values for the excluded volume parameter for PS in toluene range from w = (2.0 to 2.3Å)^3 via light scattering measured second virial coefficients to w = (3.2 Å)^3 from osmotic pressure experiments [53]. As shown in Figure 3-7, our solvated brush extensions are consistent with a larger excluded volume parameter. Such analysis offers a means to correctly estimate the molecular weight of "grafted from" chains in the absence of sacrificial chains in the reaction solution.

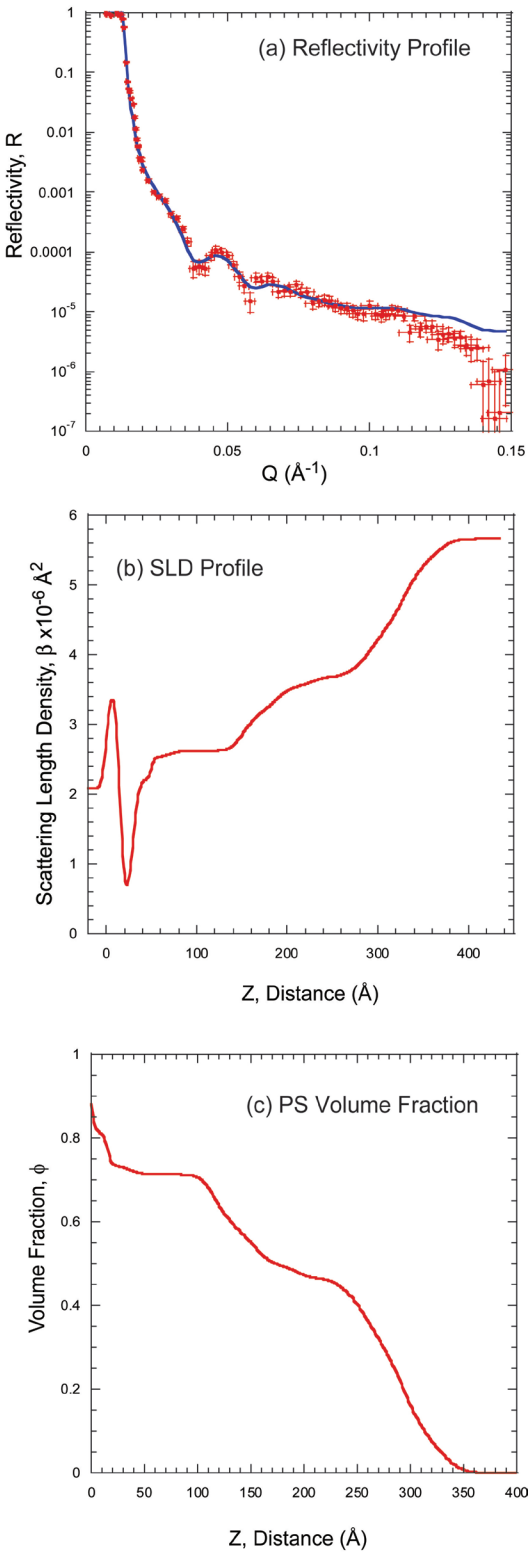

Figure 3-6 (a) Reflectivity profile for 29k PS in d-toluene. Solid curve is fit to the data based on the SLD profile shown in (b). (c) Volume fraction profile of PS.

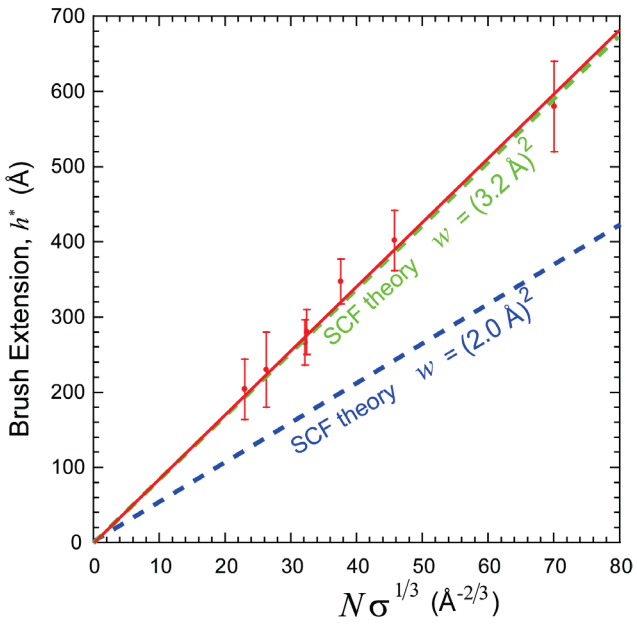

Figure 3-7 Estimated excluded volume parameter for polystyrene from brush extension.

Conclusions

Neutron reflectivity was used to study end grafted, ATRP grown PS brushes. The synthetic procedure yielded highly reproducible polymerizations and the grafted film thickness followed the MW obtained from sacrificial initiator in solution. In good solvent conditions, strongly stretched brushes of moderate molecular weight were found to maintain a parabolic density distribution consistent with theoretical predictions. The relatively high grafting density gave very high volume fractions at the substrate interface ϕ_0 (0.68-0.85). Such high volume fractions should correlate with improved wear properties and potentially lower friction in tribological applications. With increasing MW, the density distribution of the solvated brushes suggests higher density "knots" or entanglements are prevalent resulting in non-monotonic density distributions. Further studies are needed to determine if enhanced entanglements are a general feature of "grafting from" synthesis methods.

References

1. Zhao, B. and Brittain, W.J., *Polymer Brushes: Surface Immobilized Macromolecules.* Progress in Polymer Science, 2000. **25**: p. 677-710.

2. Yamamoto, S., Tsujii, Y., and Fukuda, T., *Atomic Force Microscopy of Stretching a Single Polymer Chain in a Polymer Brush.* Macromolecules, 2000. **33**: p. 5995-5998.

3. Wang, J.S. and Matyjaszewski, K., *Controlled Living Radical Polymerization - Halogen Atom Transfer Radical Polymerization Promoted by a Cu(I)/Cu(II) Redox Process.* Macromolecules, 1995. **28**(23): p. 7901-7910.

4. Wang, J.S. and Matyjaszewski, K., *Controlled Living Radical Polymerization - Atom Transfer Radical Polymerization in the Presence of Transition-Metal Complexes.* Journal of the American Chemical Society, 1995. **117**(20): p. 5614-5615.

5. Kato, M., Kamigaito, M., Sawamoto, M., and Higashimura, T., *Polymerization of Methyl Methacrylate with the Carbon Tetrachloride / Dichlorotris(triphenylphosphine)ruthenium(II) / Methylaluminum-bis-(2,6-di-tert-butylphenoxide) Initiating System - Possibility of Living Radical Polymerization.* Macromolecules, 1995. **28**(5): p. 1721-1723.

6. Solomon, D.H., Rizzardo, E., and Cacioli, P. 1986: US Patent.

7. Hawker, C.J., *Molecular Weight Control By a Living Free-Radical Polymerization Process.* Journal of the American Chemical Society, 1994. **116**(24): p. 11185-11186.

8. Chiefari, J., Chong, Y.K., Ercole, F., Krstina, J., Jeffery, J., Le, T.P.T., Mayadunne, R.T.A., Meijs, G.F., Moad, C.L., Moad, G., Rizzardo, E., and Thang, S.H., *Living Free-Radical Polymerization by Reversible Addition-Fragmentation Chain Transfer: The RAFT Process.* Macromolecules, 1998. **31**: p. 5559-5562.

9. Patten, T.E. and Matyjaszewski, K., *Atom Transfer Radical Polymerization and the Synthesis of Polymeric Materials.* Advanced Materials, 1998. **10**: p. 1-15.

10. Matyjaszewski, K. and Xia, J., *Atom Transfer Radical Polymerization.* Chemical Reviews, 2001. **101**: p. 2921-2990.

11. Hawker, C.J., *''Living'' Free-Radical Polymerization: A Unique Technique for the Preparation of Controlled Macromolecular Architectures.* Accounts of Chemical Research, 1997. **30**: p. 373-382.

12. Kamigaito, M., Ando, T., and Sawamoto, M., *Metal-Catalyzed Living Radical Polymerization.* Chemical Reviews, 2001. **101**: p. 3689-3745.

13. Devaux, C., Cousin, F., Beyou, E., and Chapel, J.P., *Low swelling capacity of highly stretched polystyrene brushes.* Macromolecules, 2005. **38**(10): p. 4296-4300.

14. Ejaz, M., Yamamoto, S., Ohno, K., Tsujii, Y., and Fukuda, T., *Controlled Graft Polymerization of Methyl Methacrylate on Silicon Substrate by the Combined Use of the Langmuir-Blodgett and Atom Transfer Radical Polymerization Techniques.* Macromolecules, 1998. **31**: p. 5934-5936.

15. Yamamoto, S., Ejaz, M., Tsujii, Y., and Fukuda, T., *Surface Interaction Forces of Well-Defined, High Density Polymer Brushes Studied by Atomic Force Microscopy. 2. Effect of Graft Density.* Macromolecules, 2000. **33**: p. 5602-5607.

16. Samadi, A., Husson, S.M., Liu, Y., Luzinov, I., and Kilbey, S.M., *Low-temperature growth of thick polystyrene brushes via ATRP.* Macromolecular Rapid Communications, 2005. **26**(23): p. 1829-1834.

17. Baum, M. and Brittain, W.J., *Synthesis of Polymer Brushes on Silicate Substrates via Reversible Addition Fragmentation Chain Tansfer Technique.* Macromolecules, 2002. **35**: p. 610-615.

18. de Boer, B., Simon, H.K., Werts, M.P.L., van der Vegte, E.W., and Hadziioannou, G., *"Living" Free Radical Photopolymerization Initiated from Surface-Grafted Iniferter Monolayers.* Macromolecules, 2000. **33**: p. 349-356.

19. Huang, W., Kim, J.-B., Bruening, M.L., and Baker, G.L., *Functionalization of Surfaces by Water-Accelerated Atom Transfer Radical Polymerization of Hydroxyethyl Methacrylate and Subsequent Derivatization.* Macromolecules, 2002. **35**: p. 1175-1179.

20. Huang, X. and Wirth, M.J., *Surface-Initiated Radical Polymerization on Porous Silica.* Analytical Chemistry, 1997. **69**: p. 4577-4580.

21. Husemann, M., Malmstrom, E.E., McNamara, M., Mate, M., Mecerreyes, D., Benoit, D.G., L., H.J., Mansky, P., Huang, E., Russell, T.P., and Hawker, C.J., *Controlled Synthesis of Polymer Brushes by "Living" Free-Radical Polymerization Techniques.* Macromolecules, 1999. **32**: p. 1424-1431.

22. Jones, D.M., Brown, A.A., and Huck, W.T.S., *Surface-Initiated Polymerizations in Aqueous Media: Effect of Initiator Density.* Langmuir, 2002. **18**: p. 1265-1269.

23. Kim, J.-B., Bruening, M.L., and Baker, G.L., *Surface-Initiated Atom Transfer Radical Polymerization on Gold at Ambient Temperature.* Journal of the American Chemical Society, 2000. **122**: p. 7616-7617.

24. Kong, X., Kawai, T., Abe, J., and Iyoda, T., *Amphiphilic Polymer Brushes Grown from the Silicon Surface by Atom Transfer Radical Polymerization.* Macromolecules, 2001. **34**: p. 1837-1844.

25. Ma, H., Davis, R.H., and Bowman, C.N., *A Novel Sequential Photoinduced Living Graft Polymerization.* Macromolecules, 2000. **33**: p. 331-335.

26. Matyjaszewski, K., Miller, P., Shukla, N., Immaraporn, B., Gelman, A., Luokala, B., Siclovan, T., Kickelbick, G., Vallant, T., Hoffmann, H., and Pakula, T., *Polymers at*

Interfaces: Using Atom Transfer Radical Polymerization in the Controlled Growth of Homopolymers and Block Copolymers from Silicon Surfaces in the Absense of Untethered Sacrificial Initiator. Macromolecules, 1999. **32**(26): p. 8716-8724.

27. Ramakrishnan, A., Dhamodharan, R., and Rühe, J., *Controlled Growth of PMMA Brushes on Silicon Surfaces at Room Temperature.* Macromolecular Rapid Communications, 2002. **23**: p. 612-616.

28. Tsujii, Y., Ejaz, M., Sato, K., Goto, A., and Fukuda, T., *Mechanism and Kinetics of RAFT-Mediated Graft Polymerization of Styrene on a Solid Surface. 1. Experimental Evidence of Surface Radical Migration.* Macromolecules, 2001. **34**: p. 8872-8878.

29. Wu, T., Efimenko, K., and Genzer, J., *Preparing High-Density Polymer Brushes by Mechanically Assisted Polymer Assembly.* Macromolecules, 2001. **34**: p. 684-686.

30. Zhao, B. and Brittain, W.J., *Synthesis of Tethered Polystyrene-block-Poly(methyl methacrylate) Monolayer on a Silicate Substrate by Sequential Carbocationic Polymerization and Atom Transfer Radical Polymerization.* Journal of the American Chemical Society, 1999. **121**: p. 3557-3558.

31. Tsujii, Y., Ohno, K., Yamamoto, S., Goto, A., and Fukuda, T., *Structure and Properties of High Density Polymer Brushes Prepared by Surface-Initiated Living Radical Polymerization.* Advances in Polymer Science, 2006. **197**: p. 1-45.

32. Sakata, H., Kobayashi, M., Otsuka, H., and Takahara, A., *Tribological properties of poly(methyl methacrylate) brushes prepared by surface-initiated atom transfer radical polymerization.* Polymer Journal, 2005. **37**(10): p. 767-775.

33. Hitchcock, P.B., Lappert, M.F., and Warhurst, N.J.W., *Synthesis and structure of a rac-tris(divinyldisiloxane)diplatinum(0) complex and its reaction with maleic anhydride.* Angew. Chem. FIELD Full Journal Title:Angewandte Chemie, 1991. **103**(4): p. 439-41 (See also Angew. Chem., Int. Ed. Engl., 1991, 30(4), 438-40).

34. Matyjaszewski, K., Miller, P.J., Shukla, N., Immaraporn, B., Gelman, A., Luokala, B.B., Siclovan, T.M., Kickelbick, G., Vallant, T., Hoffmann, H., and Pakula, T., *Polymers at Interfaces: Using Atom Transfer Radical Polymerization in the Controlled Growth of Homopolymers and Block Copolymers from Silicon Surfaces in the Absence of Untethered Sacrificial Initiator.* Macromolecules, 1999. **32**(26): p. 8716-8724.

35. Zhao, B. and Brittain, W.J., *Synthesis of Tethered Polystyrene-block-Poly(methyl methacrylate) Monolayer on a Silicate Substrate by Sequential Carbocationic Polymerization and Atom Transfer Radical Polymerization.* J. Am. Chem. Soc., 1999. **121**(14): p. 3557-3558.

36. Xia, J.H. and Matyjaszewski, K., *Controlled/''Living'' Radical Polymerization. Atom Transfer Radical Polymerization using Multidentate Amine Ligands.* Macromolecules, 1997. **30**(25): p. 7697-7700.

37. Nelson, A., *Co-refinement of multiple-contrast neutron/X-ray reflectivity data using MOTOFIT.* Journal of Applied Crystallography, 2006. **39**(2): p. 273-276.

38. Halperin, A., Tirrell, M., and Lodge, T.P., *Tethered Chains in Polymer Microstructures.* Advances in Polymer Science, 1992. **100**: p. 31-71.

39. Mark, J.E., *Polymer data handbook*. 1999, New York: Oxford University Press. xi, 1018 p.

40. Privalko, V.P., *Chain Thickness and Polymer Conformation in the Crystalline State.* Macromolecules, 1980. **13**(2): p. 370-372.

41. Milner, S.T., Witten, T.A., and Cates, M.E., *Theory of the Grafted Polymer Brush.* Macromolecules, 1988. **21**(8): p. 2610-2619.

42. Factor, B.J., Lee, L.-T., Kent, M.S., and Rondelez, F., *Observation of chain stretching in Langmuir diblock copolymer monolayers.* Physical Review E, 1993. **48**(4): p. R2354.

43. Murat, M. and Grest, G.S., *Structure of a grafted polymer brush: a molecular dynamics simulation.* Macromolecules, 1989. **22**(10): p. 4054-4059.

44. Whitmore, M.D. and Noolandi, J., *Theory of adsorbed block copolymers.* Macromolecules, 1990. **23**(13): p. 3321-3339.

45. Chakrabarti, A. and Toral, R., *Density profile of terminally anchored polymer chains: a Monte Carlo study.* Macromolecules, 1990. **23**(7): p. 2016-2021.

46. Hamilton, W.A., Smith, G.S., Alcantar, N.A., Majewski, J., Toomey, R.G., and Kuhl, T.L., *Determining the density profile of confined polymer brushes with neutron reflectivity.* Journal of Polymer Science Part B-Polymer Physics, 2004. **42**(17): p. 3290-3301.

47. Kent, M.S., Lee, L.T., Factor, B.J., Rondelez, F., and Smith, G.S., *Tethered chains in good solvent conditions: An experimental study involving Langmuir diblock copolymer monolayers.* The Journal of Chemical Physics, 1995. **103**(6): p. 2320-2342.

48. Chen, C.M. and Fwu, Y.A., *Monte Carlo simulations of polymer brushes.* Physical Review E, 2000. **63**(1): p. 011506.

49. Baranowski, R. and Whitmore, M.D., *Theory of the structure of adsorbed block copolymers: Detailed comparison with experiment.* The Journal of Chemical Physics, 1995. **103**(6): p. 2343-2353.

50. Tang, W. and Matyjaszewski, K., *Effects of Initiator Structure on Activation Rate Constants in ATRP.* Macromolecules, 2007. **40**(6): p. 1858-1863.

51. Graessley, W.W., *The entanglement concept in polymer rheology*. Advances in polymer science, v. 16. 1974, Berlin; New York: Springer-Verlag.

52. Milner, S.T., *Compressing Polymer Brushes - a Quantitative Comparison of Theory and Experiment.* Europhysics Letters, 1988. **7**(8): p. 695-699.

53. Ruths, M., Johannsmann, D., Ruhe, J., and Knoll, W., *Repulsive Forces and Relaxation on Compression of Entangled, Polydisperse Polystyrene Brushes.* Macromolecules, 2000. **33**(10): p. 3860-3870

Chapter 4: Comparison of High Density, ATRP Grown Polystyrene Brushes from Differing Initiator Lengths

Abstract

Detailed characterizations of polymer brushes prepared by atom transfer radical polymerization (ATRP) from two different self-assembled initiator layers are reported. The initiators only differed in the length of the alkyl spacer between the silane anchor and bromide terminus and reaction rates were kept constant. Both initiators yielded polystyrene brushes at ultra-high grafting densities, 0.44 or 0.56 chains/nm^2, corresponding to an initiator efficiency of 9 or 12%. Neutron reflectivity measurements were used to determine the extension and volume fraction profile of the brushes in poor and good solvent conditions. In air, a poor solvent, the dry film thickness scaled fairly linearly with chain molecular weight. In toluene, a good solvent for polystyrene, the ultra-high grafting density precluded substantial solvation resulting in polystyrene volume fractions at the initiator surface of 84% and 87%, respectively. Remarkably, parabolic brush density profiles (n=2.3 or 2.8) were still obtained.

Introduction

Grafted polymer films are widely used to modify or tailor the physical, chemical and mechanical properties of interfaces in both solid and liquid systems. Recently developed “grafting from” methods which polymerize monomers directly onto a surface from solution enable much higher grafting densities to be obtained compared to conventional “grafting to” methods. In the “grafting from approach”, a monolayer of

initiator is attached to a surface and polymerization occurs via monomer diffusion to the active sites of the growing polymer chains. This growth process can be contrasted to “grafting to” methods, in which the layer thickness must increase by diffusion of a polymer chain through the brush layer to the substrate surface. By using a "grafting-from" procedure such as Atom Transfer Radical Polymerization (ATRP), polymer brushes with much higher grafting densities can be obtained compared to conventional “grafted-to” methods such as absorption, spin coating or end-grafting via functional groups.

As brush structure depends intimately on the chain MW, solvent quality, and reduced surface density (σ^*), the ultra-high grafting densities attainable by “grafting from” methods, $\sigma^* >> 1$, may yield novel properties compared to conventional “grafted to” brushes with more modest grafting densities, $\sigma^* < 8$. For example, ATRP formed brushes have been found to have enhanced properties compared to conventional brushes including better lubrication behavior such as lower friction coefficients and increased wear resistance [1, 2]. These enhanced properties have been attributed to extremely high grafting density and strong surface anchoring of ATRP grown layers.

Structural information on ATRP films has come primarily from ellipsometry and atomic force microscopy measurements [3-5]. While these techniques are useful for estimating total thicknesses, they do not provide a detailed structural profile. Here, ATRP grown polystyrene films in good and poor solvent conditions were characterized using neutron reflectometry which provides higher resolution information of the film’s thickness, density profile, roughness, and uniformity, Figure 4-1. Because neutrons

interact with the nuclei of atoms in the film rather than electrons, radiation damage is negligible and the contrast can be enhanced by using different isotopes (i.e., H and D) while the chemistry of the materials remains unaltered. Consequently, neutron reflectometry has the potential to reveal significant relationships between the structure of the brushes and their methods of preparation.

In the reported work, a series of PS grafted silicon surfaces with varying molecular weights were prepared from two different initiator layers under identical reaction conditions. Only the residence time of the substrate in the reaction vessel was varied to control chain length. The molecular weight, grafting density, thickness, and structure of the polystyrene films were then characterized as dry films (poor solvent conditions) and as solvated brushes in a good solvent, toluene, using neutron reflectivity.

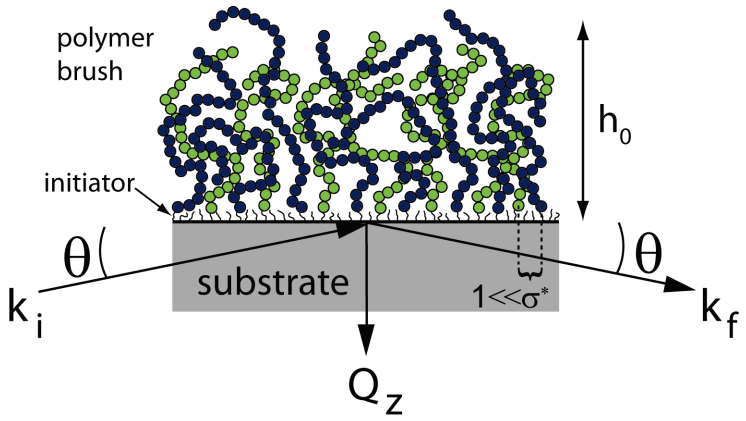

Figure 4-1 Geometry of the neutron reflectivity measurements and experimental brush system. The experimental density of the ATRP grown brushes is about twice that depicted schematically.

Experimental

Materials

All chemicals were purchased from Aldrich and Acros and used without further purification unless otherwise reported. Styrene was stirred over CaH_2 and distilled under reduced pressure to remove the inhibitor and stored under N_2 at 4°C. Copper Bromide (CuBr) was stirred in glacial acetic acid for 24 hours, washed with copious amounts of ethanol, filtered and stored under N_2 until needed. Karstedt's catalyst solution was prepared as reported by Hitchcock and Lappert [6].

Instrumentation

^{1}H and ^{13}C NMR spectra were recorded on a Varian 600 MHz instrument, and chemical shifts δ (ppm) were referenced to the residual solvent for both ^{1}H-NMR and ^{13}C NMR. FTIR measurements were conducted using a Bruker Tensor 27 equipped with a LN-MCT liquid nitrogen cooled photovoltaic detector: $350cm^{-1} – 5000cm^{-1}$ scan range with a $4cm^{-1}$ resolution, 256 scans in transmission mode, using neat films on NaCl plates. All advancing and receding contact angles were measured using the sessile drop method with an Advanced Surface Technology Products, Inc. VCA Optima XE goniometer and Milli-Q water (18MΩ/cm) with a drop size of 2.5μL dispensed for advancing and 1.0μL retracted for receding angles were used. Number average molecular weights (M_n) and polydispersity indices (PDI) were determined using a gel-permeation chromatography apparatus (GPC) with THF solvent at 25°C with a flow rate of 1.00 mL/min. A Thermoseparation Products P-100 isocratic pump, autosampler, three Polymer Standards Service columns (100Å. 1000Å, and linear), Knauer refractive index detector were connected in series and calibrated using polystyrene standards (Polymer Standards

Service, M_p = 400-1,000,000; PDI = 1.10). Atomic force microscopy (AFM) images were collected on a Digital Instruments Nanoscope III in tapping mode under ambient conditions using silicon cantilevers (spring constant 0.58 N/m). RMS roughness and feature dimensions were calculated with the AFM manufacturer's provided software on (5 μm x 5 μm) scan size images. Statistical analysis was also performed on each image using full width at half maximum with each data point and heights where determined using the AFM manufacturer's program.

Synthesis of allyl-2-bromoisobutyrate

Synthesis was carried out by John R. Ell, PhD Chemistry, University of California, Davis, 2008

Allyl alcohol was vacuum distilled using a Vigreux fractionating column and stored under N_2 and molecular sieves until needed. Allyl alcohol (15 mL, 218 mmol) in dry DCM (150 mL) was stirred vigorously under a balloon of N_2 in a three neck 250 mL round bottom flask at 0 ºC. Dry triethylamine (36.4 mL, 261 mmol) was slowly injected into the reaction flask. The reaction mixture was stirred for 10 min at 0ºC. 2-Bromoisobutyrate bromide (28.7 mL, 239 mmol) in dry DCM (10 mL) was then added dropwise through an addition funnel, and the solution was stirred for 5 hours at room temperature. Precipitated salts were removed by filtration then DI water (100 mL) was added. The resulting solution was extracted with DI water (3 x 100 mL), 1M HCl (3 x 100 mL), saturated sodium bicarbonate (1 x 100mL), and saturated NaCl (1 x 100mL). The organic extract was dried by stirring over anhydrous Na_2SO_4 for 10 min before it was filtered and the solvent removed *in vacuo*. The resulting pale yellow liquid was vacuum distilled (200 mTorr at 25 ºC), which yielded a clear liquid (43.1 g, 96%). ^{1}H NMR:

($CDCl_3$) δ (ppm) 1.95 (6H, s), 4.67 (2H, d), 5.27-5.41 (2H, dd), 5.91-5.97 (1H, m). ^{13}C NMR: ($CDCl_3$) δ (ppm) 30.9, 55.8, 66.5, 118.6, 131.1, 171.4 FTIR: ν (cm^{-1}) 3088, 2987, 2932, 1741.5, 1649.

Synthesis of (3-trichlorosilyl)allyl-2-bromoisobutyrate Surface Bound Initiator

An oven dried 50 mL Schlenk flask was charged with a stir bar and allyl-2-bromoisobutyrate (15.0 g, 72.9 mmol) then evacuated and back-filled with N_2 (3x). Karstedt's catalyst (200 μL, 2.5 wt%) was injected and the reaction was cooled to 0ºC. Trichlorosilane (TCS) (11.1 mL, 109.35 mmol) was injected into the reaction flask under a stream of N_2. The solution was allowed to warm to room temperature and then was heated for 5 h at 30 ºC. Warning! [A possible violent exothermic reaction occurs upon warming to room temperature never use a sealed flask unless pressure glassware is used as well as a blast shield for protection]. Volatiles were removed under reduced pressure and the solution was cooled and then immediately transferred to a round bottom flask and vacuum distilled at 40 mTorr and 53 °C, which yielded (10.7g, 71 %) as a clear liquid. ^1H NMR: ($CDCl_3$) δ (ppm) 1.51 (2H, t), 1.94 (6H, s), 1.9-2.0 (2H, m), 4.23 (2H, t). ^{13}C NMR: ($CDCl_3$) δ (ppm) 20.7, 21.8, 30.9, 55.8, 66.3, 171.6 FTIR: ν (cm^{-1}) 2987, 2932, 2879, 1740. The (3-trichlorosilyl) allyl-2-bromoisobutyrate is subsequently referred to as the "short" initiator.

Detailed information regarding the synthesis and characterization of the (3-trichlorosilyl)allyl-11-undecane bromoisobutyrate (referred to as "long" initiator) is found in the previous chapter.

ATRP Initiator Deposition Procedure and Characterization

The ATRP initiator was deposited on Si substrates using a slight modification to literature procedure[7]. The Si wafers were washed with copious amounts of acetone, isopropyl alcohol, and Milli-Q water, dried under a stream of N_2, then immediately UVO etched. The substrates were subsequently immersed in a 2 mM solution of the ATRP initiator (50 μL), in dry toluene (100 mL) and stirred for 1 hour then removed, and rinsed in fresh toluene [8]. The substrates were baked at 80 °C for 2 h. After baking, the water contact angle of the Si wafers coated with the short initiator film was 81.4 ± 0.5° for Si wafers. A smooth monolayer resulted with RMS roughness (5 μm^2 area) = 0.30 nm and R_{max} (5 μm^2 area) = 3.1 nm. The water contact angle of the long initiator film was 80.8 ± 0.7°. A smooth monolayer resulted with RMS roughness (5 μm^2 area) = 0.90 nm and R_{max} (5 μm^2 area) = 5.0 nm.

Preparation of ATRP Grafted PS Chains

PS brushes were grafted from the ATRP initiator in a custom reaction flask made to accommodate the large substrates (50mm diameter) required for neutron reflectivity measurements. The reaction flask was charged with CuBr (124 mg, 0.846 mmol), $CuBr_2$(10 mg, 0.0432 mmol), and the ATRP functionalized substrate which acted as sacrificial surface to measure brush thickness. The flask was then evacuated and back-filled with N_2 (3x). In a separate Schlenk flask, that was also evacuated and back-filled with N_2 (3x), the styrene (10 mL, 86.4 mmol), anisole (7 mL), and ebib (13 μL, 0.09 mmol) as the sacrificial initiator were added then degassed using three freeze / pump / thaw cycles in liquid N_2. The solution along with sparged PMDETA (189 μL, 0.907 mmol) was injected into the flask and stirred at 90°C for a specified amount of time.

The time to achieve a given molecular weight was estimated using calibration reactions, which used identical conditions but in the absence of a surface. Samples were taken every hour via a purged syringe to determine the molecular weights (M_n) and thereby the approximate time to terminate the brush growth for a desired molecular weight. The monomer conversion and the M_n of free chains in the supernatant were determined using GPC.

The polymerization was terminated by removing the heat source, exposing the reaction to air and diluting the reaction solution with copious amounts of THF. The PS grafted substrates were washed (3x) with 100 mL of THF at 65 °C for 1 h and then at 50 °C for 24 h each to remove any residual polymer, and stored in airtight containers until used. Contact angle (91.5± 3.2 º), thickness (53.9 nm ± 0.089 nm), RI = 1.57, RMS (1 μm^2 area) = 0.54 nm and R_{max} (1 μm^2 area) = 6.8 nm was determined. ATRP: St : ebib : CuBr : $CuBr_2$: PMDETA : Anisole = 960 : 1 : 1 : 0.05 : 1.05 : 40 v/v%

Neutron reflectivity measurements

Neutron reflectivity measurements were performed on the time-of-flight SPEAR beamline at the Manuel Lujan Neutron Scattering Center, Los Alamos National Laboratory. The range of neutron wavelengths was λ=2-16Å. The measured Q_Z range, was from 0.008 to about 0.11Å^{-1} and reflectivities, R, with reasonable statistics can be obtained to values of R~10^{-6}. The error bars on the data represent the statistical errors in the measurements (standard deviation, δR) where the uncertainty in the Q_Z resolution, ΔQ_Z / Q_Z, was nearly constant over this scattering vector range with a value of ~3%. The data were fit with nonlinear least-squares regression using the MOTOFIT reflectivity analysis package or MIRROR program developed by Hamilton and described in Chapter 1, which are both based on the iterative, dynamical method.

Results and discussion

Single surface measurements in air: Poor solvent conditions

The neutron reflectivity profiles from typical ATRP polystyrene brushes grown on silicon substrates from the two different initiators in air are shown in Figure 4-2. Both shown PS brushes have a M_n=23k. The fitted SLD profile consisted of several layers: silicon substrate, 15-25Å native oxide, polystyrene, and air. These layers were modeled as boxes of constant thickness and SLD. Interfaces were smeared with an error function. For the (3-trichlorosilyl)allyl-11-undecane bromoisobutyrate samples (long initiator), a 15-20Å layer with a SLD of 0.4x10^{-6}Å^{-2} was required to obtain a good fit to the reflectivity data. This is consistent with the expected thickness of 21Å based on chemical structure [9]. In contrast, a discrete initiator layer was not required for samples grown from the (3-trichlorosilyl)allyl-2-bromoisobutyrate samples (short initiator). For both

types of films, the SLD of the polymer layer converged to $1.45x10^{-6}Å^{-2}$ compared to the expected value of $1.42x10^{-6}Å^{-2}$ for bulk PS, thus lending credence to the quality of the polymerization. Atomic force microscopy (AFM) showed uniform topography of the films in air with an RMS roughness of 0.5 nm (5µm x 5µm scan size) .

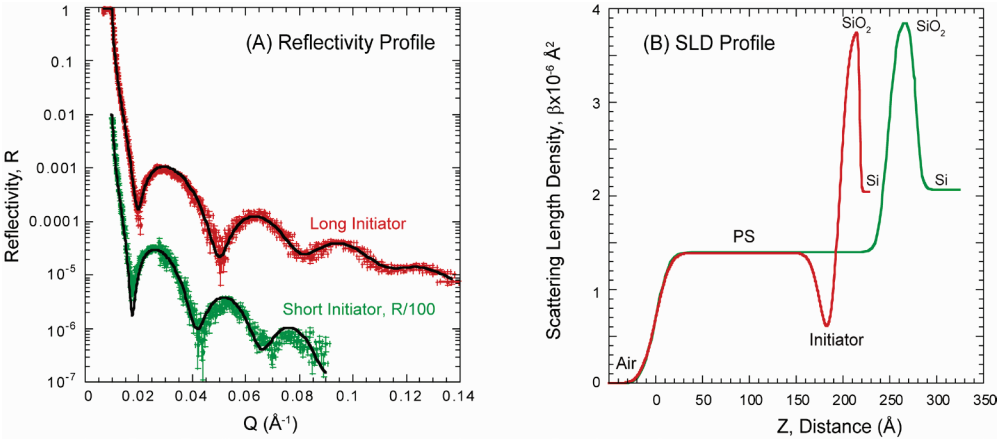

Figure 4-2 (A) Reflectivity profiles for 23k MW PS films grown from the two different initiators. The short initiator profile is decreased by 2 orders of magnitude for clarity. Line fits to the data are based on the SLD profiles shown in (B).

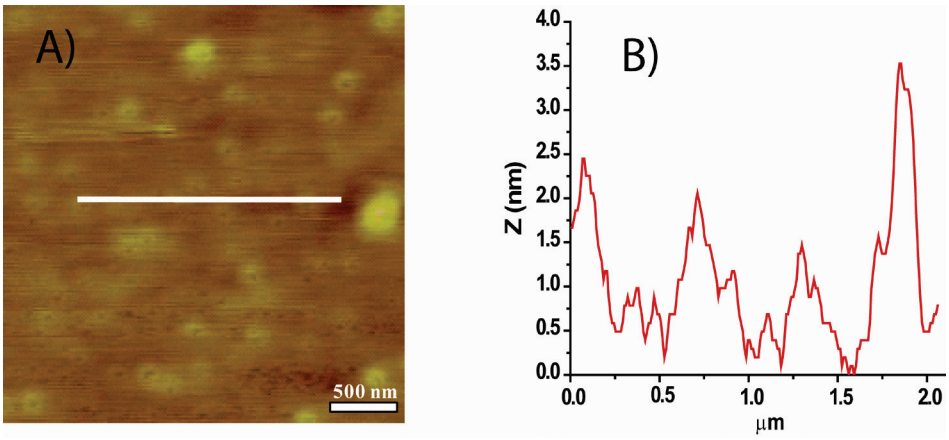

Figure 4-3 A) AFM of PS from long initiator and B) determined roughness

Figure 4-4 shows a summary plot of the dry thickness, *t*, of the PS layers in air versus molecular weight. The thickness of the films was obtained by neutron reflectivity measurements. The molecular weight was obtained from GPC measurements of free polymer chains created from sacrificial initiator in the reaction supernatant during the polymerization of each sample. For both initiators, the PS film thickness scales fairly linearly with molecular weight demonstrating that the initiator layers and reaction conditions reproducibly initiate chain growth with the same grafting density. The linearity also strongly suggests that the molecular weight of the grafted chains correlates well to that found for sacrificial initiator chains growing in solution [10]. The grafting density was determined by fitting the equation $t = (\sigma / \rho N_A) M_n$ to the results in Figure 4-4. Using a bulk PS density of ρ = 1.05 g/cm^3 [11], the average grafting density was calculated to be 0.44±0.03 chains/nm^2 for the long initiator and 0.56±0.04 chains/nm^2 for the short initiator. The cross sectional area of a single polystyrene chain in the crystalline state is 0.7 nm^2 [12], which yields a theoretical maximum grafting density of 1.4 chains/nm^2.

The overall efficiency of the initiators can also be obtained from the grafting density of the polymer films. The cross-sectional area [13, 14] of an aminopropylsilane molecule in a self-assembled monolayer is approximately 0.21nm^2. Using this value, the efficiency of the initiator reaction was 9 and 12%, respectively for the long and short initiators. Based on a monomer repeat length of 2.6Å [15], the chain extension in air ranges from 25 to 31% for the long initiator and from 32 to 48% for the short initiator. As shown in Figure 4-4, very high extensions of the initiator grown films occurred at relatively low molecular weights and tended to decrease as the polymerization index

increased. This finding suggests that more chain termination events occur as the polymerization progresses.

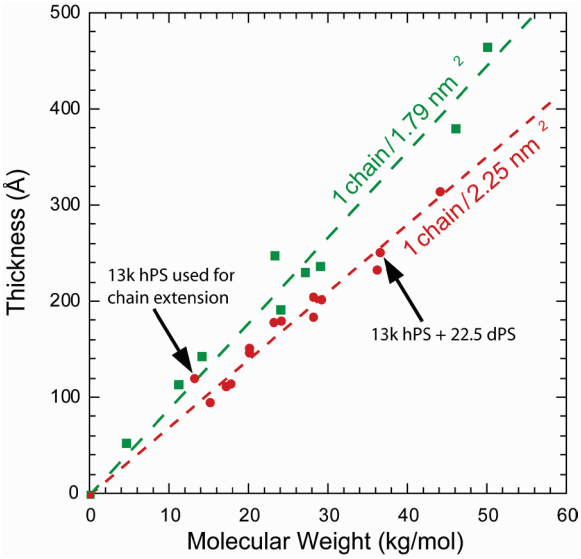

Figure 4-4 Thickness of dry PS films as a function of MW for the two initiators.

Chain extension measurements in air

An advantage of living polymerizations is the ability to carry out chain extensions with different monomers to create grafted, multi-block copolymer chains. Figure 4-5 shows the results of PS diblock film where the polymerization was initially done with hydrogenated styrene monomer and then continued with deuterated styrene (dPS). Diblock extensions could be easily carried out when the monomer was diluted to 50% by volume with toluene. Attempts to chain extend in bulk styrene monomer were much less successful.

For the initial film, 13k hPS, the polymerization is higher than expected, but lower initiator efficiency is obtained with the chain extension of 22.5k dPS as marked in Figure 4-4. This again suggests that more chain termination events occur as the polymerization progresses.

The SLD profile in Figure 4-5B was converted to a volume fraction profile of each block (Figure 4-5C) using:

$$SLD_{fitted} = \phi_{hPS}(SLD_{hPS}) + (1 - \phi_{hPS})SLD_{dPS} \quad \textbf{Equation 4-1}$$

$$\phi_{dPS} = 1 - \phi_{hPS} \quad \textbf{Equation 4-2}$$

The resulting volume fractions do not exhibit two well defined layers but a mixture of both hPS and dPS with about 85% hPS and 15% dPS at the initiator layer. There are two possible explanations. First, the dPS chain extended off of the end of the hPS block and there is mixing of the two blocks. Second, since only 9-12% of the initiator molecules initiate to grow the first block, it is possible the dPS chain started on the active initiator sites on the substrate. The second scenario is unlikely as it is precisely the steric hindrance of the originally growing hPS blocks that inhibit those initiator molecules from polymerizing in the first place. In addition, the total dry film thickness of 35.5k PS molecular weight is in good agreement with the linear trend line for the long initiator (Figure 4-4). Finally, poor chain extension was observed when pure styrene monomer was used as the reaction solution. Good chain extension was obtained only when the monomer was diluted with toluene vs. theta solvent monomer. This suggests that access to the reactive chain ends is a limiting factor.

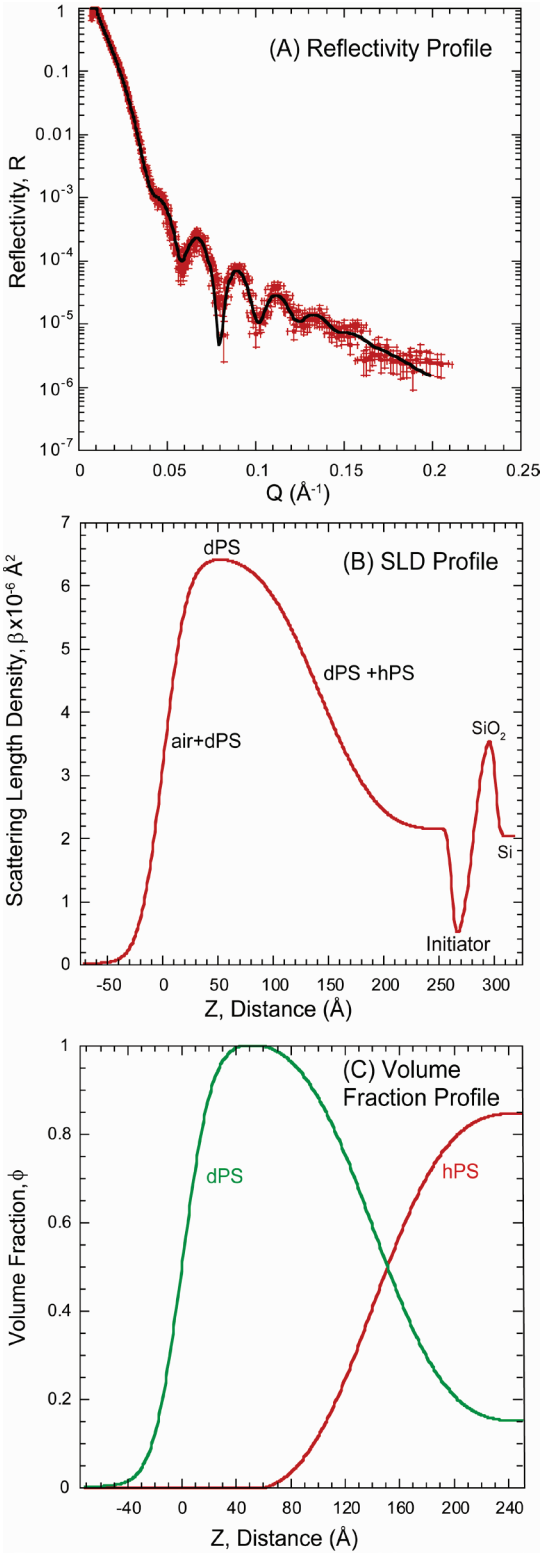

Figure 4-5 (A) Chain extension reflectivity profile for long initiator hPS 13k + dPS 22.5k. Solid line is fit to the data based on the SLD profile shown in (B). (C) is the volume fraction profile of each.

Surface measurements in deuterated toluene: Good solvent conditions

Figure 4-6 shows the reflectivity profile of the same 23k PS layers in Fig 4-2, but in deuterated toluene, a good solvent for PS. To extract the polymer density distribution, the brush was modeled as a power law extending from the initiator layer (Eq 4-2), smoothed by a reversed power law (Eq 4-3) accounting for the polymer tails extending into the solvent (Eq 4-4).

$$SLD(0 \leq x \leq h_1) = SLD(0) - [SLD(0) - SLD(h_1)]\left(\frac{x}{h_1}\right)^n \quad \textbf{Equation 4-2}$$

$$SLD(h_1 \leq x \leq h_2) = SLD(h_2) + [SLD(h_1) - SLD(h_2)]\left(\frac{h_2 - x}{h_2 - h_1}\right)^n \quad \textbf{Equation 4-3}$$

$$SLD(x \geq h_2) = SLD_{solvent} \quad \textbf{Equation 4-4}$$

where x=0 corresponds to the portion of the brush extending from the initiator layer, h_1 the endpoint of the first (n_1) power law, and h_2 the endpoint of the second (n_2) reversed power law starting the bulk deuterated toluene layer. An identical model was used in Chapter 2, Eq 1. Deuterated toluene – C_8D_8 has a theoretical neutron SLD of 5.66 x 10^{-6} $Å^{-2}$, however, in some cases the solvent was partially hydrogenated, Figure 4-6B. In contrast to SLD models completed in air, a short initiator layer was required to obtain a reasonable fit. This layer is much thicker and rougher than the long initiator sample suggesting that the layer is not single smooth monolayer and pulls away from the surface under solvation.

To obtain the polymer brush density distribution, the SLD profiles (Fig. 4-6C) were converted to volume fraction profiles using

$$SLD_{fitted} = \phi_{PS}(SLD_{PS}) + (1 - \phi_{PS})SLD_{toluene}$$ **Equation 4-5**

An important check of the physical reasonableness of the model fit was verified by conservation of mass where the amount of polymer in the solvated case matched to ±2% that found in the dry case.

The volume fractions were fit using a power law profile (Eq 1-1) with parameters summarized in Table 4-1. Even for very high grafting coverages studied here for the short and long initiators, 33 and 45 times the overlap concentration, the unconfined brush density profile was found to remain roughly parabolic (n=2.3 or 2.8). Such high grafting densities appear to preclude toluene penetration, yielding polystyrene volume fractions of 84% and 87% at the initiator surface.

For comparison, just the dried hPS volume fraction from the previous chain extended diblock is shown as well. The resulting profile is surprisingly parabolic (n=2.4) and the volume fraction at the initiator surface is nearly identical to the long initiator brush in a good solvent.

Table 4-1 Properties of Solvated Brushes

Initiator	$M_n \cdot 10^{-3}$ (g/mol)	PDI	h_{dry} (Å)	σ^*	ϕ_0	h_0(Å)	n
Long	23	1.05	180	33	0.84	260	2.4
Short	23	1.22	248	45	0.87	340	2.8

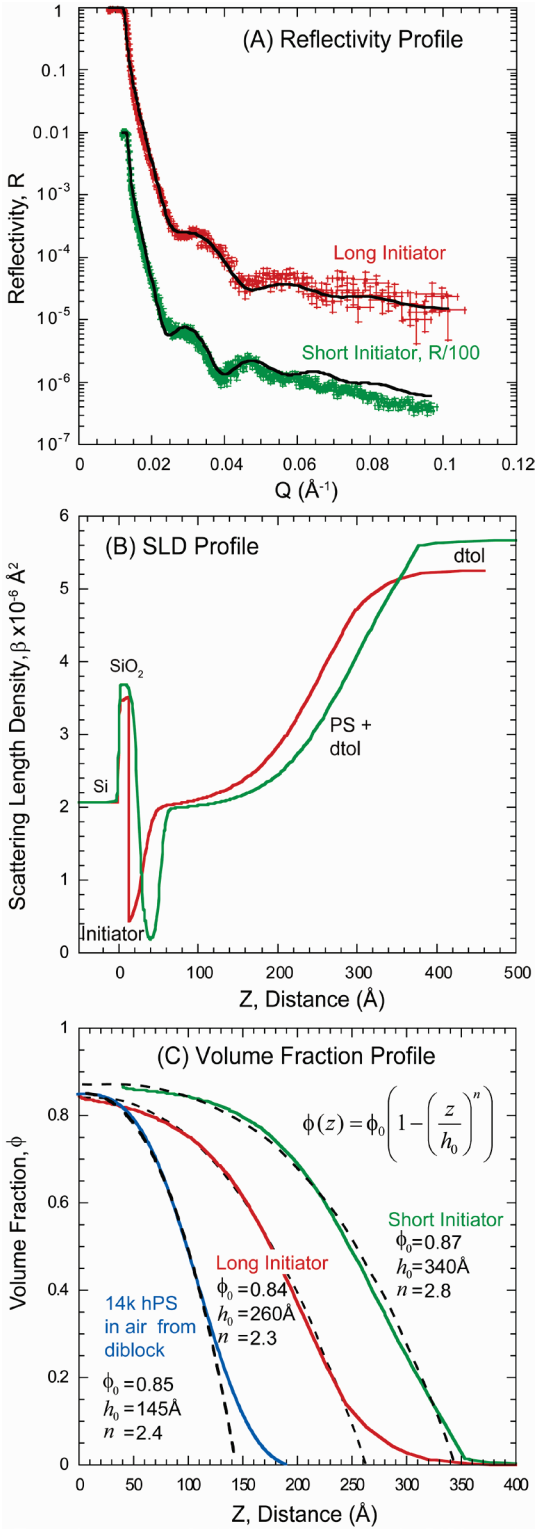

Figure 4-6 (A) Reflectivity profile for 23k PS films in d-toluene. The short initiator profile is decreased by 2 orders of magnitude for clarity. Line fits to the data are based on the SLD profiles shown in (B). (C) Volume fraction profiles of PS with power law fits (dashed).

Conclusions

Neutron reflectivity was used to study end grafted, ATRP grown PS brushes using two different initiator lengths. The procedure yielded highly reproducible polymerizations and the grafted film thickness followed the MW obtained from sacrificial initiator in solution. At relatively low molecular weights, there is a slight decrease in the linearity of thickness vs. MW as the polymerization index increased suggests that more chain termination events occur as the polymerization progresses. Each initiator had differing but fairly consistent grafting densities of 0.44 or 0.56 chains/nm^2 for the short and long initiator, respectively. Potentially other grafting densities can be controlled with differing initiator lengths. Chain extensions of the hPS layers with dPS when the monomer was diluted with 50% toluene were successfully grown with a total thickness following the same total MW trend for that initiator.

In good solvent conditions, strongly stretched brushes of moderate molecular weight were found to maintain a parabolic density distribution consistent with theoretical predictions. Additionally, the short initiator layer was much thicker and rougher than the short initiator suggesting that the short initiator is not a smooth monolayer and pulls away from the surface as the polymer is solvated. The relatively high grafting density gave very high volume fractions at the substrate interface ϕ_0(0.84 and 0.87). Such high volume fractions should correlate with improved wear properties and potentially lower friction in tribological applications.

References

1. Kobayashi, M. and Takahara, A., *Synthesis and frictional properties of poly(2,3-dihydroxypropyl methacrylate) brush prepared by surface-initiated atom transfer radical polymerization.* Chemistry Letters, 2005. **34**(12): p. 1582-1583.

2. Sakata, H., Kobayashi, M., Otsuka, H., and Takahara, A., *Tribological properties of poly(methyl methacrylate) brushes prepared by surface-initiated atom transfer radical polymerization.* Polymer Journal, 2005. **37**(10): p. 767-775.

3. Borner, H.G., Beers, K., Matyjaszewski, K., Sheiko, S.S., and Moller, M., *Synthesis of molecular brushes with block copolymer side chains using atom transfer radical polymerization.* Macromolecules, 2001. **34**(13): p. 4375-4383.

4. Pyun, J., Kowalewski, T., and Matyjaszewski, K., *Synthesis of polymer brushes using atom transfer radical polymerization.* Macromolecular Rapid Communications, 2003. **24**(18): p. 1043-1059.

5. Chen, J.Z., Zhao, Q.L., Lu, H.C., Huang, J., Cao, S.K., and Ma, Z., *Polymethylene-b-Polystyrene Diblock Copolymer: Synthesis, Property, and Application.* Journal of Polymer Science Part a-Polymer Chemistry, 2010. **48**(9): p. 1894-1900.

6. Hitchcock, P.B., Lappert, M.F., and Warhurst, N.J.W., *Synthesis and structure of a rac-tris(divinyldisiloxane)diplatinum(0) complex and its reaction with maleic anhydride.* Angew. Chem. FIELD Full Journal Title:Angewandte Chemie, 1991. **103**(4): p. 439-41 (See also Angew. Chem., Int. Ed. Engl., 1991, 30(4), 438-40).

7. Pasetto, P., Blas, H.l.n., Audouin, F., BoissieÌ€re, C.d., Sanchez, C.m., Save, M., and Charleux, B., *Mechanistic Insight into Surface-Initiated Polymerization of Methyl Methacrylate and Styrene via ATRP from Ordered Mesoporous Silica Particles.* Macromolecules, 2009. **42**(16): p. 5983-5995.

8. Edmondson, S. and Huck, W.T.S., *Controlled growth and subsequent chemical modification of poly(glycidyl methacrylate) brushes on silicon wafers.* Journal of Materials Chemistry, 2004. **14**(4): p. 730-734.

9. Akgun, B., Uğur, G.k.e., Brittain, W.J., Majkrzak, C.F., Li, X., Wang, J., Li, H., Wu, D.T., Wang, Q., and Foster, M.D., *Internal Structure of Ultrathin Diblock Copolymer Brushes.* Macromolecules, 2009. **42**(21): p. 8411-8422.

10. Halperin, A., Tirrell, M., and Lodge, T.P., *Tethered Chains in Polymer Microstructures.* Advances in Polymer Science, 1992. **100**: p. 31-71.

11. Mark, J.E., *Polymer data handbook*. 1999, New York: Oxford University Press. xi, 1018 p.

12. Privalko, V.P., *Chain Thickness and Polymer Conformation in the Crystalline State.* Macromolecules, 1980. **13**(2): p. 370-372.

13. von Werne, T. and Patten, T.E., *Atom Transfer Radical Polymerization from Nanoparticles: A Tool for the Preparation of Well-Defined Hybrid Nanostructures and for Understanding the Chemistry of Controlled/"Living" Radical Polymerizations from Surfaces.* Journal of the American Chemical Society, 2001. **123**(31): p. 7497-7505.

14. Brittain, W.J., Boyes, S.G., Granville, A.M., Baum, M., Mirous, B.K., Akgun, B., Zhao, B., Blickle, C., and Foster, M.D., *Surface rearrangement of diblock copolymer brushes - Stimuli responsive films*, in *Surface- Initiated Polymerization Ii*. 2006, Springer-Verlag Berlin: Berlin. p. 125-147.

15. Devaux, C., Cousin, F., Beyou, E., and Chapel, J.P., *Low Swelling Capacity of Highly Stretched Polystyrene Brushes.* Macromolecules, 2005. **38**(10): p. 4296-4300.